Journal of Energy Chemistry 44 (2020) 73–89

Contents lists available at ScienceDirect

Journal of Energy Chemistry

journal homepage: www.elsevier.com/locate/jechem

http://www.journals.elsevier.com/journal-of-energy-chemistry/

Review

Three dimensional porous frameworks for lithium dendrite suppression

Shuyan Ni[1], Shuangshuang Tan[1], Qinyou An*, Liqiang Mai*

State Key Laboratory of Advanced Technology for Materials Synthesis and Processing, Wuhan University of Technology, Wuhan 430070, Hubei, China

ARTICLE INFO

Article history:
Received 17 May 2019
Revised 18 September 2019
Accepted 24 September 2019
Available online 1 October 2019

Keywords:
Lithium metal battery
3D porous frameworks
Lithium dendrite
Lithium sulfur batteries
Lithium oxygen batteries
Li plating/stripping

ABSTRACT

Lithium metal is a promising anode material owing to its very low electrochemical potential and ultrahigh specific capacity. However, the growth of lithium dendrites could result in a short lifespan, low coulombic efficiency, and potential safety hazards during the progress of lithium plating/stripping. These factors drastically hinder its application in lithium metal batteries. This review focuses on the use of three dimensional (3D) porous host frameworks to improve Li plating/stripping behaviors, accommodate the change in volume, and suppress or block lithium dendrite growth. Various 3D porous frameworks, including the conductive carbon-based, metal-based, and lithiophilic inorganic-compound frameworks are introduced and summarized in detail. The particular functions, relative developments, and optimized strategies of various 3D porous frameworks for lithium deposition/dissolution behaviors are discussed. Moreover, the challenges and promising developments in the field of Li metal anodes will be discussed at the end of this review.

Shuyan Ni is an undergraduate student of Materials Science and Engineering at Wuhan University of Technology. Her current research focuses on Li metal batteries.

Shuangshuang Tan received his B.S. degree in Material Science and Engineering from Wuhan University of Technology in 2016. He is currently working toward the Ph.D. degree and his current research focuses on rechargeable multivalent ion batteries and Li metal batteries.

Qinyou An is Associate Professor of Materials Science and Engineering at Wuhan University of Technology (WUT). He received his Ph.D. degree from WUT in 2014. He carried out his postdoctoral research in the laboratory of Prof. Yan Yao at the University of Houston in 2014-2015. Currently, his research interest includes energy storage materials and devices.

Liqiang Mai is Chang Jiang Scholar Chair Professor of Materials Science and Engineering at Wuhan University of Technology (WUT). He received his Ph.D. from WUT in 2004 and carried out his postdoctoral research in Prof. Zhonglin Wang's group at Georgia Institute of Technology in 2006-2007. He worked as an advanced research scholar in Prof. Charles M. Lieber's group at Harvard University in 2008-2011 and Prof. Peidong Yang's group at University of California, Berkeley in 2017. His-current research interests focus on new nanomaterials for electrochemical energy storage and micro/nano energy devices.

1. Introduction

Lithium ion batteries have been commonly used for electricity storage owing to their high energy density and long cycling performance. They revolutionized transportation and communications by

* Corresponding authors.
E-mail addresses: anqinyou86@whut.edu.cn (Q. An), mlq518@whut.edu.cn (L. Mai).
[1] These authors contributed equally to this work.

https://doi.org/10.1016/j.jechem.2019.09.031

making possible the development of mobile phones, camcorders, and even electric vehicles [1,2]. Among all the options for lithium-storage anodes, lithium metal is an ideal choice owing to its very high theoretical capacity (by mass, 3860 mAh g^{-1}) and low electrochemical potential of –3.04 V [3,4]. The development of a safe lithium metal anode is a key technology to commercialize high-energy lithium metal battery systems, including lithium sulfur and lithium air batteries [5–10].

However, the undesired lithium dendrite growth during the progress of Li plating/stripping has always been the major cause of safety and aging issues of Li metal batteries. It has been discovered that lithium dendrite growth is self-enhanced, and multiple models have been proposed to illustrate this phenomenon. First, Barton et al. verified that the spherical tips of Li deposition exhibit high electric and ionic fields, and thus, Li^+ ion deposition occurs primarily on the protrusions. Therefore, the dendrite growth rate is determined by tip radius [11–13]. Moreover, Dollé et al. proposed that the crystalline defect is the key factor to dendrite growth, and it includes weak points on the solid electrolyte interphase (SEI), grain boundaries, dislocations, and contaminants [14,15]. When lithium dendrites grow to a certain extent, they may penetrate the separator and connect with the cathode, causing cell short circuit, fire, and even blast. If the lithium dendrites break, "dead lithium" will be formed, leading to rapid capacity fading. Moreover, the deposited Li metal easily reacts with the electrolyte and forms fresh interfacial film, which increases the anode polarization and results in low coulombic efficiency [16–21].

Based on the above growth mechanisms of Li dendrites, many promising methods have been proposed to suppress the undesired electrochemical behavior, including liquid electrolyte modification [22–25], solid-state electrolyte [26–29], artificial SEI [30–45] (including fluorinated SEI [35–40] and sulfurized SEI [41–45]), and nanostructured frameworks [46,47]. Liquid electrolyte modification improves significantly the ionic conductivity, but most liquid electrolytes can react with the fresh Li dendrites, leading to low coulombic efficiency [48]. The solid-state electrolyte is relatively stable against Li metal and can overcome the electrolyte leak issue and flammability feature. Most importantly, its high modulus can efficiently block Li dendrite growth. However, it has unsatisfactory ionic conduction and high interface impedance [49,50]. Infiltrating a Li metal anode into three dimensional (3D) framework matrixes is a more universal method, employed in various Li metal batteries owing to its lower influence on battery performance and lower matching requirements to other battery components. The 3D framework can effectively suppress lithium dendrite growth by dramatically decreasing the local electric field and blocking the vertical growth toward the cathode. Meanwhile, it mitigates the change in volume of the Li metal owing to its porous structure and high surface area [4,51,52]. The detailed advantages are as follows:

(1) The high specific surface area of 3D nanostructures improve Li metal utilization significantly, changing the Li^+ ion diffusion path from two dimensional (2D) to 3D, thus enhancing the rate of performance [53–55]. Meanwhile, the electrolyte could permeate easily into the frameworks, narrowing the Li^+ ion concentration boundary layer and decreasing the voltage polarization of the anode. Then, the impedance will be decreased, leading to a remarkably increased charge/discharge rate [56]. Moreover, the large pore volume can accommodate the large expansion/shrink of the lithium metal anode, reducing the formation of “dead lithium” and improving the cycling stability.
(2) High mechanical strength, shear module, and elastic strength. The 3D frameworks tend to be constructed with low-dimensional nanomaterials. It is observed that intercalation-induced stress would occur in large particle sizes under high discharge current densities. Therefore, to reduce the intercalation-induced stress during cycling, smaller particles with larger aspect ratios should be synthesized [57]. Besides, when certain stress is applied, the 3D frameworks avoid stress concentration and bear the stress evenly. Therefore, they possess higher ultimate strength than the bulk Li metal.

Herein, we review the various 3D porous frameworks based on their conductive and lithiophilic properties for a Li metal anode. These 3D frameworks with different geometric configurations, physical properties, and chemical surfaces induce the lithium metal to uniformly deposit on specific locations (Fig. 1). The corresponding coulombic efficiencies and overpotentials of these composited Li anodes are listed in Table 1, and radar plots of each category are summarized (Fig. 2). It can be concluded that the metal-based and carbon-based frameworks have more advantages in terms of cost and conductivity, while the conductive composite and lithiophilic frameworks exhibit better cycle life and lower overpotentials. The details of the structure design method, dendrite suppression theories, and enhanced electrochemical performance will be introduced and summarized. The challenges and promising developments of 3D frameworks for the Li metal anode will be prospected at the end of this review.

2. Fabrication of Li-host composite electrode

A Li-host composite electrode is commonly used to pre-store Li into a 3D host electrode; thus, Li plating/stripping can be more efficient, the volume change can be mitigated, and the anode space can be predefined. Major methods to obtain a Li-host composite electrode generally include melting infusion [58–60], electrochemical deposition [61,62, and mechanical rolling [63–65]].

In the melting infusion method, Li metal is heated to its melting point in an anaerobic atmosphere and is infused into a framework that possesses good Li affinity. The molten Li metal can be well entrapped into the framework and remain stable, but the demanding conditions of high temperature and an anaerobic atmosphere require a complex production process and high costs. Electrochemical deposition, which is mostly carried out by assembling coin cells, is the most common way to prepare a Li-host electrode. However, it lacks control of the Li deposition progress, which could cause uneven Li deposition on the surface and dendrite formation. In addition, with this method, large-scale fabrication is not feasible. By pressing the metallic Li to the framework under rolling pressure, the Li metal can fill its voids and form a composite structure. This mechanical rolling method is a facile method that can be operated at room temperature to fabricate Li-host composite electrodes at a large scale. However, it may not be effective for suppressing lithium dendrites and reducing polarization. All of the current methods face some issues in particular applications owing to their high cost or unsatisfactory performance of the obtained electrodes. Novel methods to store Li metal in a practical and effective way are required, with a high degree of control of size, thickness, and flatness.

3. Conductive 3D framework

The Li ion concentration and the Li^+-deposited electric field play critical roles in Li plating morphology during the lithium plating and stripping processes as Li ions are combined with electrons to dissolve into the electrolyte in the stripping process. Therefore, a conductive framework could be used to regulate this Li metal deposition and dissolution process. Sand’s time is usually used to describe the initiation time of dendrite growth in the dilute solution,

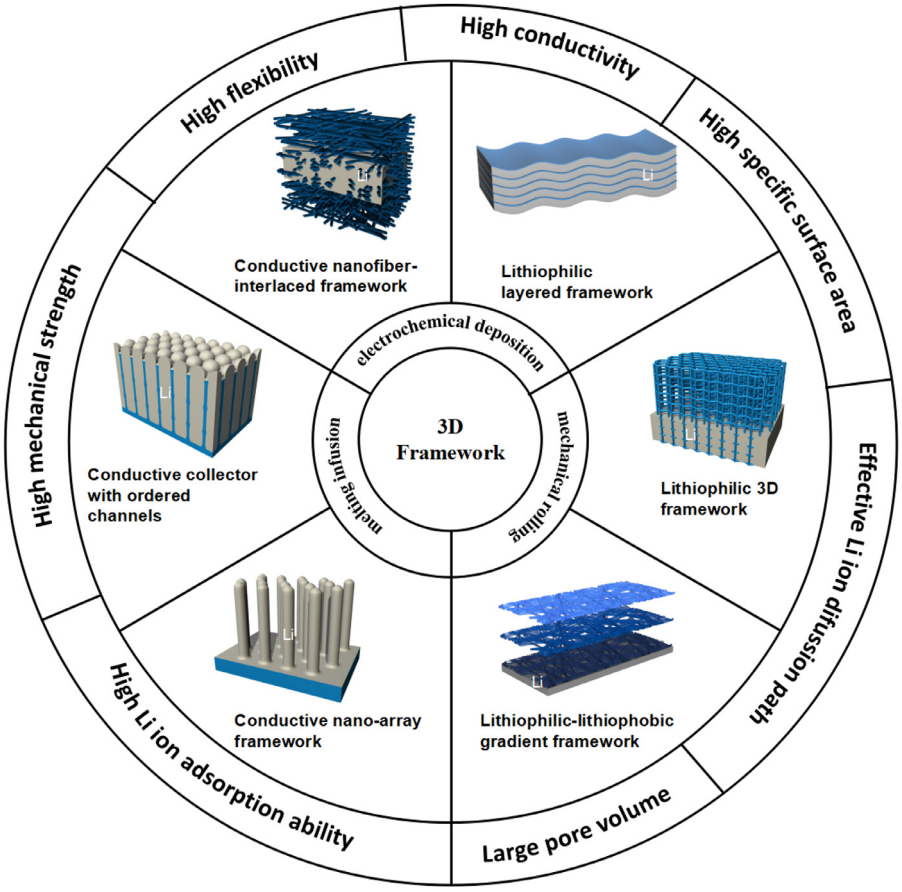

Fig. 1. Schematics of lithium plating on different frameworks.

Table 1. Coulombic efficiency (CE) and overpotential of different 3D frameworks for Li metal anode.

3D framework/Li electrode	CE (%)/current density (mA cm^{-2})/lifespan (cycles)	Overpotentials (mV)/current density (mA cm^{-2})/time (h)	Ref.
Metal-based frameworks			
Cu nanowire current collector	97.6/2/50	20/1/550	[66]
Porous Cu/CF framework	98/1/270	27/0.5/620	[67]
Cu skeleton current collector	98.5/0.5/50	50/0.2/600	[68]
3D Cu current collector by chemical dealloying	97/1/140	50/0.2/1000	[69]
Cu current collector with vertically aligned microchannels	98.5/1/200	20/1/200	[70]
Polyimid-clad Cu grid current collector	96/0.5/150	100/0.2/500	[71]
Fibrous metal felt framework	99.5/1.64/200	–	[72]
Carbon-based frameworks			
Carbon nanowire 3D framework	99.5/2/300	–	[73]
Graphitized carbon fiber current collector	98/2/50	20/2/300	[74]
Lotus-root like carbon matrix with Nafion	98/8/80	15/1/700	[75]
Graphene nested carbon fiber cloth current collector	98.5/1/70	25/2/500	[46]
3D carbon nanofiber interlayers	95/0.5/100	40/0.5/500	[76]
Polyrotaxane Binders/carbo nanotubes	98.1/1/250	–	[92]
Wrinkled graphene cages	99/1/140	–	[94]
Conductive composite frameworks			
Gold nanoparticles pillared rGO	98.7/0.5/200	25/0.5/1600	[77]
Graphene/carbon nanotube	99.6/2/225	–	[78]
$Li_{6.4}La_3Zr_2A_{l0.2}O_{12}$ nanoparticles /CNFs scaffold	98/3.5/30	80/5/1000	[79]
Lithiophilic frameworks			
Li-coated polyimide matrix with ZnO shell	–	40/1/100	[58]
Layered Li–rGO electrode	–	200/3/100	[60]
3D glass fibers	98/0.5/90	37/0.5/90	[62]
Porous carbon/Si matrix	–	90/3/13	[80]
N-doped binder network	98/0.5/350	–	[81]
Li/C with –NH functional group anode	89/1.56/1000	–	[82]
Lithiophilic–lithiophobic gradient framework	–	25/1/1000	[83]
Porphyrin framework with lithiophilic sites	98/1/300	20/1/300	[114]
Binary lithium–aluminum alloy layer	98.6/2/85	25/1/1450	[124]
Au/Ni/Al_2O_3 gradient framework	98.1/1/500	50/2/1750	[137]

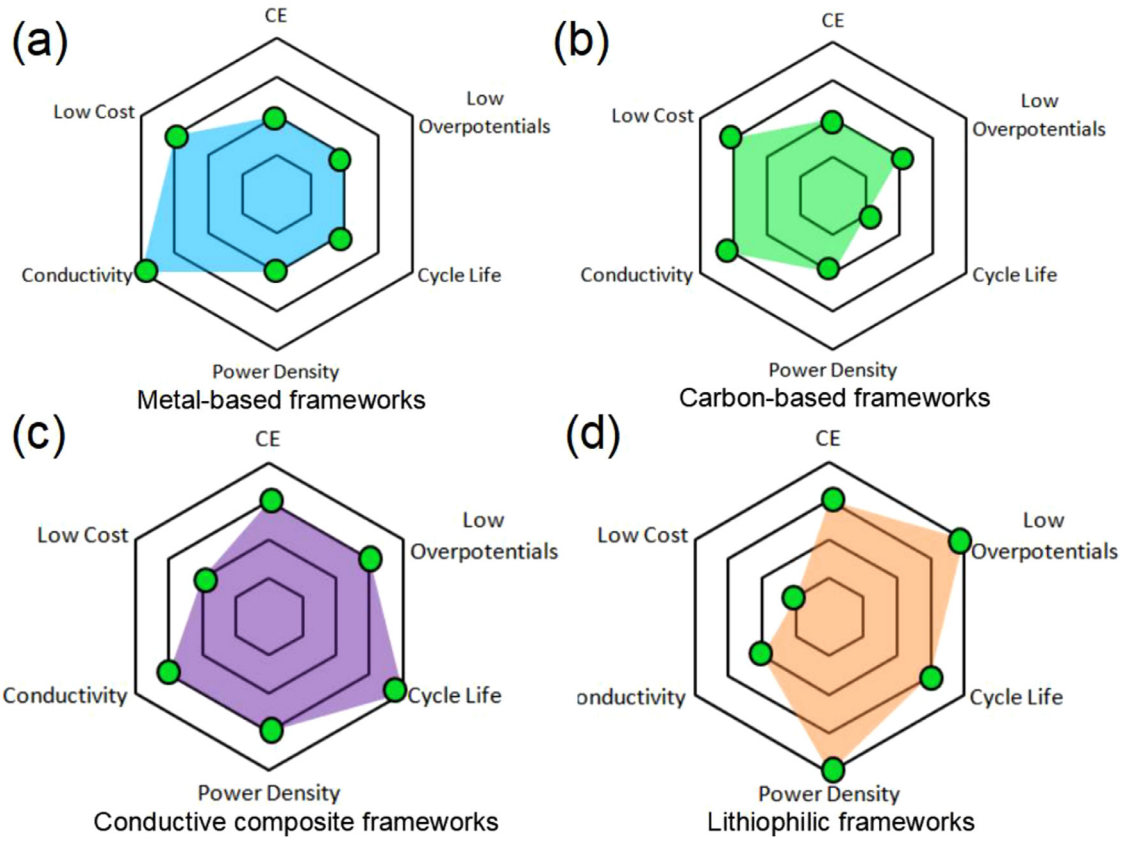

Fig. 2. Radar plots of the electrochemical performance, conductivity and cost of (a) metal-based frameworks, (b) carbon-based frameworks, (c) conductive composite frameworks, and (d) lithiophilic frameworks. The charting of CE, overpotentials, cycle life, power density and conductivity is based on statistics from Table 1, and the cost rating is mainly based on the cost of raw material and the production condition.

from Eq. (1) [84].

$$\tau = \pi D\left(\frac{eC_0}{2Jt_a}\right)^2 \quad (1)$$

where τ is the time when lithium dendrites start to grow, D is the ambipolar diffusion coefficient, e is the electric charge, C_0 is the initial lithium ion concentration, J is the effective electrode current density, and t_a is the number of anionic transference. The 3D conductive framework offers high electroactive surface area, dramatically reducing the real area current density J. Thus, the start time of Li deposition is delayed, extending the lifespan of the Li metal battery. Besides, the 3D conductive framework offers a homogeneous electric field distribution. It can form a strong and even electric field to make Li^+ ions plate on the whole surface of the framework instead of a single tip or edge, thus controlling the uniform distributions of Li plating. By designing an ordered and porous conductive framework for Li^+ plating/stripping, lithium dendrites can be effectively inhibited, and the cycle life of the battery can be notably enhanced. Among them, the metal-based and carbon-based frameworks have been most widely studied.

3.1. Metal-based 3D framework

The metallic framework exhibits better electron transfer and higher mechanical properties compared with the carbon-based or other 3D framework materials. Moreover, most metal-based structures can act as a current collector and a lithium insertion framework. The current collector is decisive to the plated Li morphology because it affects Li plating nucleation during the initial period. Thus, the construction of a 3D metal current collector structure to induce uniform deposition of Li metal is the focus of many researchers [66,67,85]. Conventional current collectors have defects such as kinks, terraces, and steps, where the stronger electric fields result in more concentrated Li nucleation. This uneven Li nucleation causes further dendrite growth [86–88]. A 3D submicron skeleton current collector was reported by Yang et al. [68]. (Fig. 3a, b). In this structure, Li is deposited on the 3D Cu skeleton current collector and is inserted into its pores owing to the uniform electric field distribution, thereby suppressing Li dendrite growth. In this case, the lithium metal anode displayed a coulombic efficiency of 98.5% with low voltage hysteresis. Further, the percentage of Li metal deposition inside the 3D structure (η) was proposed as Eq. (2):

$$\eta = \frac{r-1}{r} \quad (2)$$

where r is the ratio of the electrode's electroactive surface area to geometric area. As shown in Fig. 3(c), when $r=1$ (2D planar current collector), η=0, suggesting that all the Li atoms deposit on the geometric surface of the current collector. Assuming that $r=8.8$, η is calculated as 88.6%, which indicates that 11.4% of Li is deposited outside of the 3D current collector. Hence, a high electroactive area ratio is the critical factor for the 3D current collectors to effectively accommodate Li metal.

According to the above-mentioned theory, tuning the pore sizes inside the metal current collector to regulate the electroactive area ratio may be an effective way to control the Li deposition behavior. Yun et al. investigated the influence of various pore sizes on the lithium dendrite formation by comparing the 2D planar Cu (less micro-pores), porous Cu current collector (pore size ranging from ≈200 nm to ≈2 μm), and the commercial Cu foam (pore size

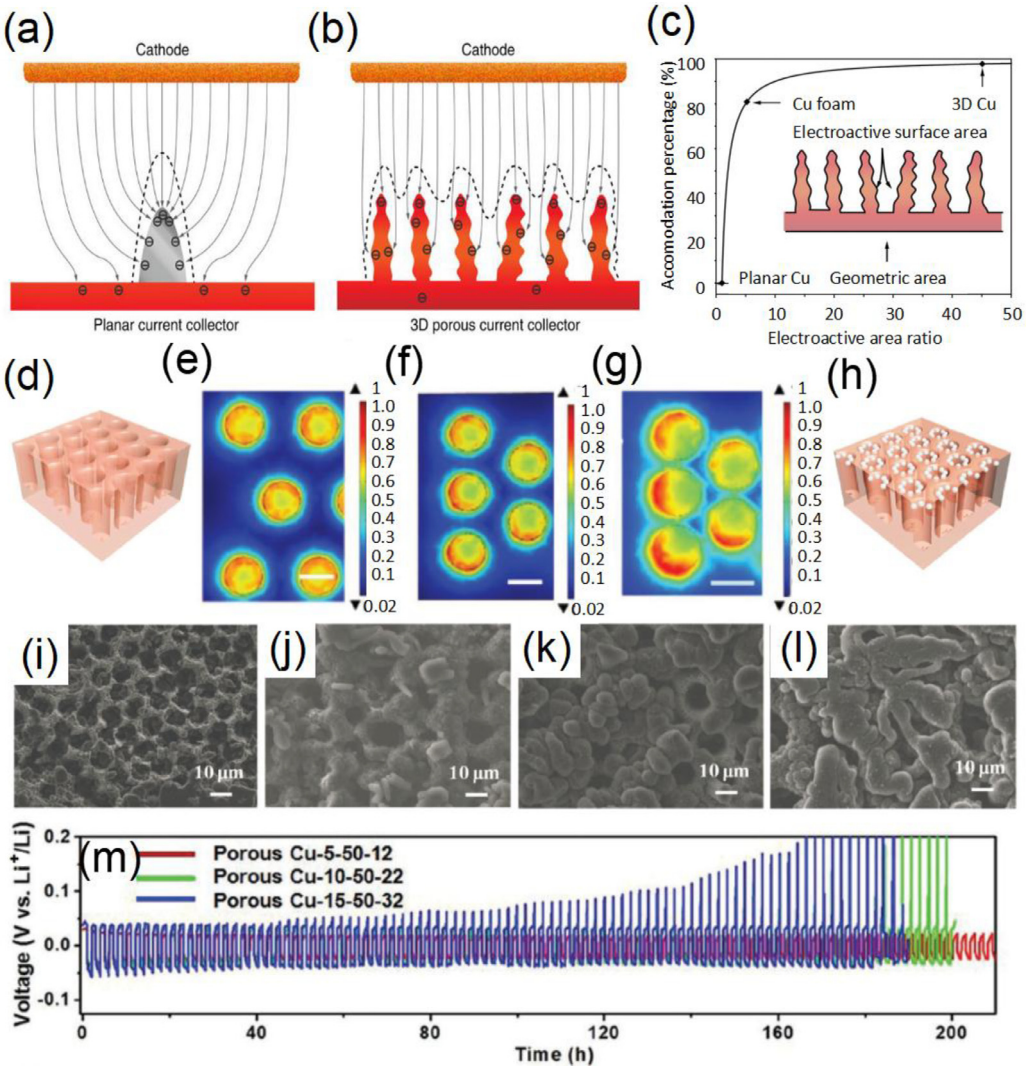

Fig. 3. Schematic of Li metal deposition on (a) planar Cu current collector and (b) 3D Cu current collector. (c) Li accommodation percentage with electroactive area ratio. Reprinted with permission from Ref. [68]. Copyright (2014) Published by WILEY-VCH Verlag GmbH & Co. KGaA, Weinheim. (d) Schematic of Cu current collector with vertically aligned microchannels. (e–g) Current density distribution simulation of the surface of Cu-pore size-depth-spacing, Cu-5-50-20 (e), Cu-5-50-16 (f), Cu-5-50-12 (g); the scale bars in the images are of 10 μm. (h) Schematic of Li deposition inside the microchannels. (i-l) SEM images of Li metal deposition on the Cu microchannels with the radii of 5 μm (i), 7.5 μm (j), 10 μm (k), and 15 μm (l). (m) Galvanostatic cycling performance of porous Cu symmetric cells. Reprinted with permission from Ref. [70]. Copyright (2017) Published by WILEY-VCH Verlag GmbH & Co. KGaA, Weinheim.

ranging from ≈100 to ≈400 μm) [69]. They found that if the pores are too small (micro-pores), they cannot confine the dendrite growth and Li metal is more likely to deposit on the surface of the current collector. If the pores are too large (macro-pores), they cannot provide enough electrical surface for the Li. Thus, Li deposition cannot be regulated and would grow in the macro-pores uncontrollably, forming Li dendrites and dead Li. As a result, pore sizes ranging from ≈200 nm to ≈2 μm inside the current collector are the appropriate choice for suppressing the Li dendrite growth. The specific pore size, pore depth, and pore spacing of porous Cu current collectors were further discussed by Wang et al. (Fig. 3d-m) [70]. They pointed out that the Cu current collector with microchannels can improve the safety of lithium anodes (Fig. 3d, h). Samples with a pore spacing (the distance between two adjacent circle centers) of 20, 16, and 12 μm were stimulated using the COMSOL Multiphysics stimulation, where porous Cu-5–50–12 stood for porous Cu with a pore radius of 5 μm, a pore depth of 50 μm, and a pore spacing of 12 μm. The stimulation showed that the inner surface of the microchannels exhibited larger current density than that on the upper surface of porous Cu (Fig. 3e-g); thus, Li preferred to nucleate inside the channels. These results are consistent with the lightning rod theory [86,89], which states that the electric charge density in high curvature areas is significantly larger than others. The Li deposition morphology on the porous Cu with different radii was compared (Fig. 3i-l). Scanning electron microscopy (SEM) images showed the worse restriction effect of porous Cu for Li deposition with the increasing pore radius. Therefore, Cu-5–50–12 was shown to have the lowest current density. Thus, in a Cu current collector with appropriate pore size, additional modifications can be made to ensure that Li dendrites cannot penetrate through the separator. A polyimide (PI)-clad copper grid current collector for Li metal anodes was designed [71], where the upper PI layer physically blocked the Li dendrites from protruding and the pinholes in the upper PI layer made way for sufficient electrolyte diffusion. In this way, Li metal could be homogenously deposited inside the hollow compartments without dendrite formation after long-term cycling.

Aside from the Cu current collector, there are other metals such as Li [90], Ni, and fibrous metal felt that can be used to modify

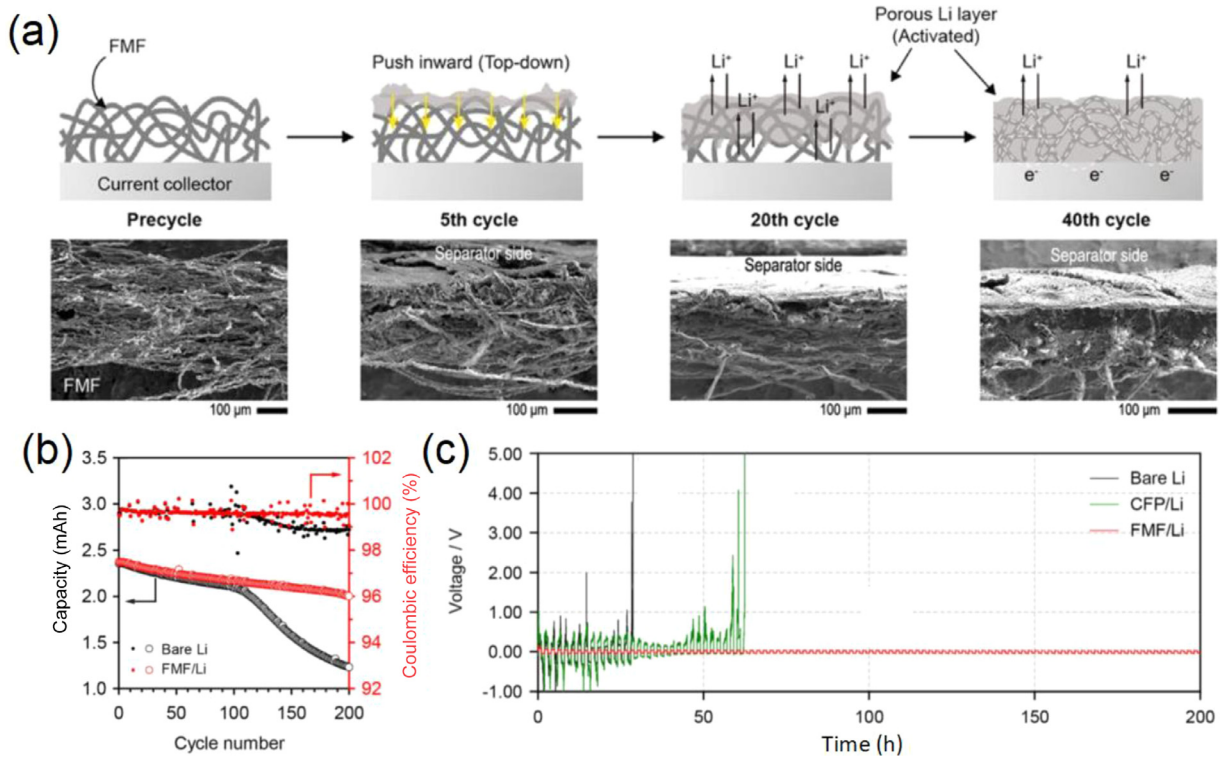

Fig. 4. (a) Schematic and corresponding SEM images of FMF electrodes during the Li half-cell cycling test. (b) Cycling performances and coulombic efficiency at a 1 C-rate (1.64 mA cm^{-2}). (c) Time-voltage profiles of the coin-type Li|Li symmetric cells with the bare Li, carbon fiber paper/Li, and FMF/Li electrodes at 10 mA cm^{-2}. Reprinted with permission from Ref. [72]. Copyright (2016) Published by Nature Publishing Group.

the anode. Lee et al. presented a fibrous metal felt (FMF) [72] as an interlayer to modulate the Li/electrolyte interfacial structure (Fig. 4a). The FMF framework has good mechanical robustness, flexibility, and chemical and electrochemical stability with areal density equal to that of a 11 μm-thick Cu foil, which makes it a fine current collector. It also provides sufficient space for Li^+ passage through the intervals between the metal fibers. As a result, the FMF electrode exhibited a coulombic efficiency of 99.5% after 200 cycles (Fig. 4b) and a small overpotential of 30 mV for more than 100 cycles at 10 mA cm^{-2} (Fig. 4c). Compared to the above porous Cu matrixes with elaborate nano-engineering, the construction of the FMF interlayer is more feasible and practical to improve the cell performances as it does not require a pre-lithiation process, and thus, it can be further applied in advanced Li battery systems as the anode material. Therefore, the 3D FMF interlayer is more commercially viable.

Although metal-based 3D frameworks exhibit great conductivity and mechanical strength, most of them are heavy, thus adding mass to the whole battery and further lowering the specific energy density. Moreover, metal-based frameworks with ordered pores require a complex fabrication processing, which involves high costs. These major flaws need to be improved to apply them in the industry.

3.2. Carbon-based 3D framework

In earlier studies, carbon nanowire/nanofiber (CNF) 3D frameworks were frequently used to suppress the lithium dendrite growth owing to their good conductivity, porosity, and facile preparation [47,76,91,92]. A common way is modifying the Cu current collector by a 3D CNF network, as proposed by Zhou et al. (Fig. 5a) [73]. The CNF networks were prepared by polymer graphitization and a simple vacuum filtration method. When Li metal was deposited into CNF networks, no dendrite was observed, thereby leaving a flat surface morphology. This CNF/Li networks delivered a coulombic efficiency of 99.9% for more than 300 cycles. Therefore, 3D CNFs provided abundant reaction sites and void spaces for Li insertion and deposition. Meanwhile, the areal current densities were effectively reduced and distributed uniformly, leading to a no dendrite behavior. Moreover, 3D CNFs networks could be used to cover both sides of the separator for blocking the penetration of lithium dendrites, so that Li^+ ions could be guided to homogenously deposit along the fibers to avoid Li dendrite growth.

The 3D CNF frameworks that possess high strength and light weights could be applied as a stable and low-cost current collector, which helps reduce the mass of the inactive component, compared with the metal current collectors [93]. Zuo et al. demonstrated a 3D current collector constituted by self-sustaining graphitized carbon fibers (GCF) (Fig. 5b) [74]. The GCF electrode exhibited high surface area and porous structure, which led to low current density and no obvious Li dendrite formation after 300 h at 2 mA cm^{-2} with low voltage hysteresis, thus resulting in high coulombic efficiency and a long lifespan (Fig. 5c).

Compared with carbon nanofibers, carbon nanotube (CNT) is a hollow structure that has an inner and outer surface. During the diffusion process of Li atoms, the nanotube structure exhibits a drifting effect owing to the structural stresses, which slows down the Li diffusion kinetics inside the nanotube. As a result, the Li atoms prefer to deposit on the internal surface. Xiang et al. investigated Li metal deposition behaviors in CNT with various internal to external radius ratios (R_0:R_1) ranging from 8:10 to 1:10 (Fig. 6a) [75]. As observed by the SEM images of CNT after Li deposition at 1 mAh, it was found that as R_0:R_1 reduced, Li atoms were preferentially deposited on the interior surface (Fig. 6b-d). Following this pattern, a lotus-root like carbon matrix (LCNF) with parallel channels (~50 nm) was formed by uniform Li deposition (Fig. 6e). The LCNF structure guided Li ions to deposit on the interior surface of the channels, while the carbon shell mechanically

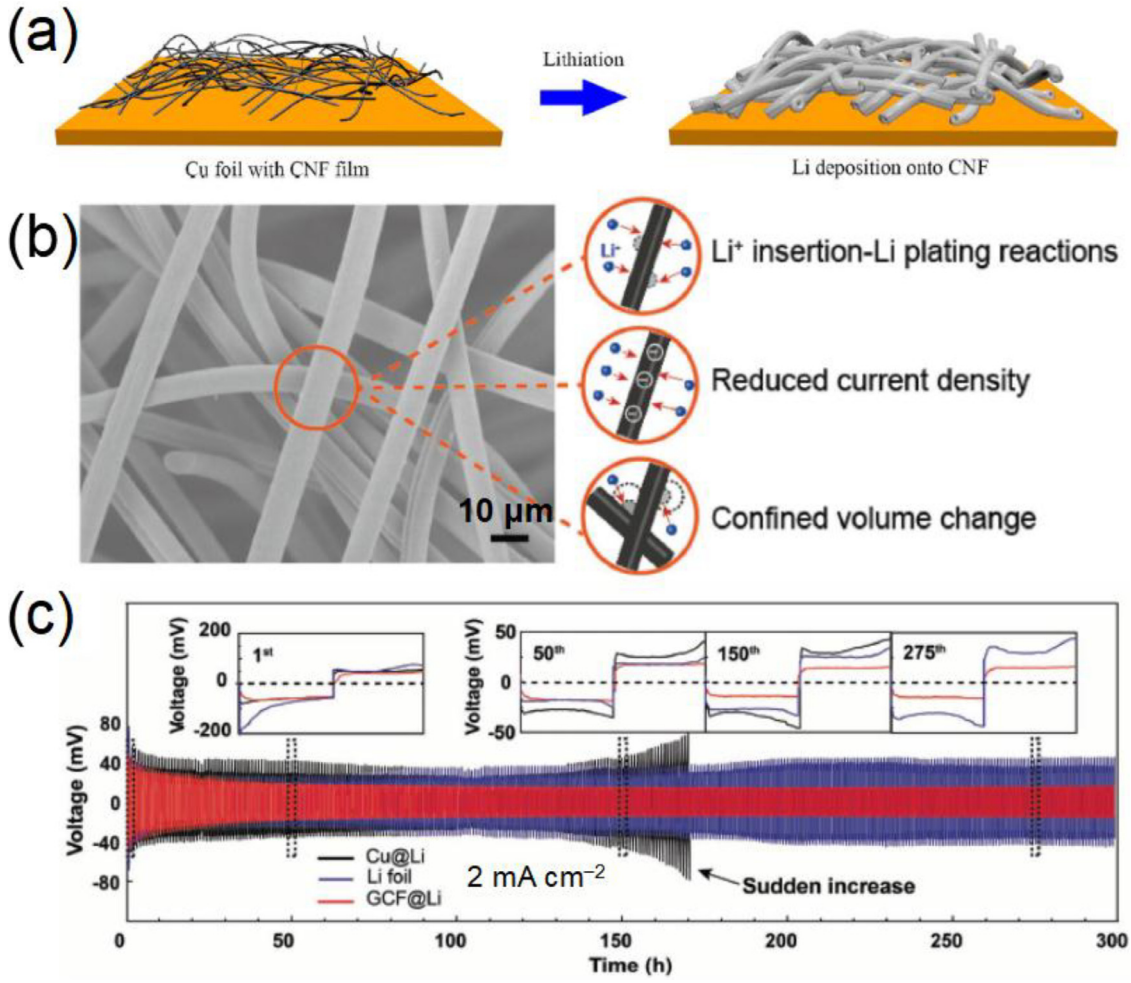

Fig. 5. (a) Schematic of Li deposition on Cu foil with CNFs film. Reprinted with permission from Ref. [73]. Copyright (2016) Published by Springer Nature Switzerland AG. Part of Springer Nature. (b) SEM image and schematic of GCFs. (c) Galvanostatic cycling performance of Cu@Li, Li foil, and GCF@Li symmetric cells. Insets are the detailed voltage profiles of the 1st, 50th, 150th, and 275th cycles, respectively. Reprinted with permission from Ref. [74]. Copyright (2017) Published by WILEY-VCH Verlag GmbH & Co. KGaA, Weinheim.

prevented the dendrite from protruding. This multichannel structure endowed the LCNF anode with a low polarization of ~15 mV, high stability of 700 h without an increase in polarization, and a high CE of 98% at current densities of 5 and 8 mA cm^{-2} (Fig. 6f).

Graphene network is another efficient porous framework because it not only can trap lithium metal in the framework to suppress dendrite growth, but also serve as a 2D orderly conductive network [94,95]. Mukherjee et al. introduced an anode with porous graphene networks (PGN) synthesized by applying thermal shock to graphene oxide paper (Fig. 7a) to make the graphene lattice defects act as seed points to start Li plating [96]. Li plating behaviors were observed on the interior and exterior surface of the electrode. It was observed that Li metal plated within pores that were few tens of nanometers on the interior of the electrode, and thus, dendrites were confined within these pores. No dendrite was observed on the exterior surface area as the exterior surface was relatively small, thus restraining the amount of Li that can be deposited on it (Fig. 7b). In this way, Li metal mostly plated on the inner surface of the electrode. Thereby, Li dendrite growth was prevented, and a steady discharge capacity of 915 mAh g^{-1} with an average coulombic efficiency as high as 99% is achieved (Fig. 7c). Other graphene networks, such as porous carbon generated from asphalt [97] and layered reduced graphene oxide [60], also make use of this feature to accomplish Li deposition control.

Carbon-based frameworks are easy to fabricate and modify, and thus, they can act as current collector, separator, or other components of the Li metal battery. Meanwhile, the high conductivity, flexibility, and light weight property of carbon greatly enhances the performance of the composited Li anode. However, doping modification or defects easily occur during the synthetic process, which significantly reduces its conductivity, although an enhanced Li^+ adsorption ability is exhibited. When these carbon-based frameworks with defects are commercially applied as the current collectors, for example, they would exhibit a large interface impedance between the current collector and battery case or external circuit. Therefore, the carbon-based frameworks as current collector and Li plating matrix need further research for their use as commercial Li metal battery.

3.3. Conductive composite 3D framework

By combining the high conduction of metals and the flexibility and light weight of carbon materials, some 3D metal–carbon composite frameworks may display comprehensive functions for more uniform and stable Li plating and lower polarization in Li metal batteries. The pure reduced graphene oxide (rGO) film as Li plating matrix would exhibit a limited inducing ability, leading to a possible Li deposition atop the rGO film during the ultralong Li plating/stripping processes. Metal particles can be used

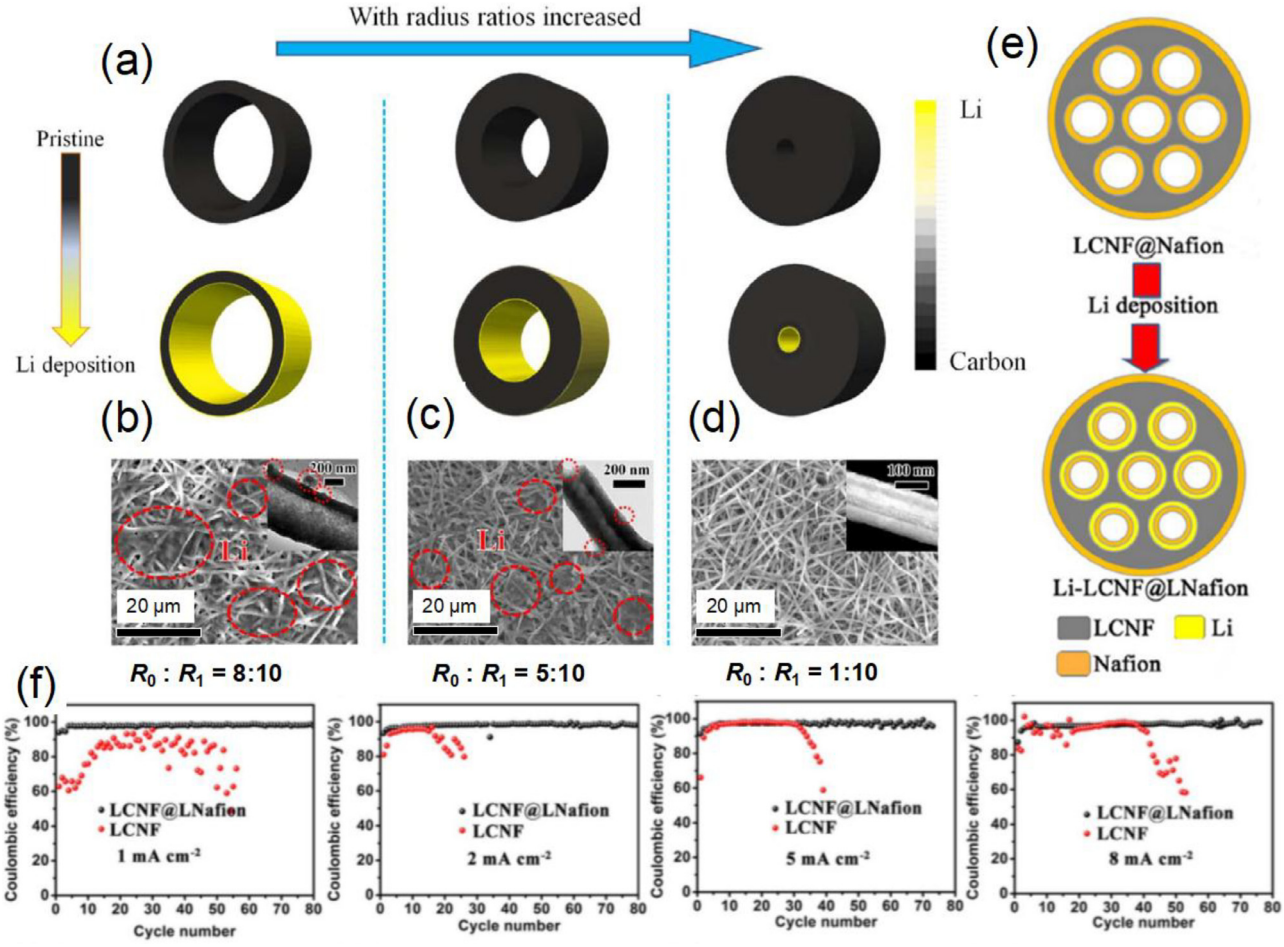

Fig. 6. Schematic (a) and SEM images of carbon nanotubes with different inner and outer radius (R_0:R_1) ratios at 1 mAh: (b) 8:10, (c) 5:10, (d) 1:10. The insets are the corresponding TEM images. (e) Schematic of Li deposition on LCNF@Nafion. (f) Coulombic effciency of the LCNF@LNafion electrode at 1, 2, 5, 8 mA cm^{-2}. Reprinted with permission from Ref. [75]. Copyright (2017) Published by Elsevier Ltd.

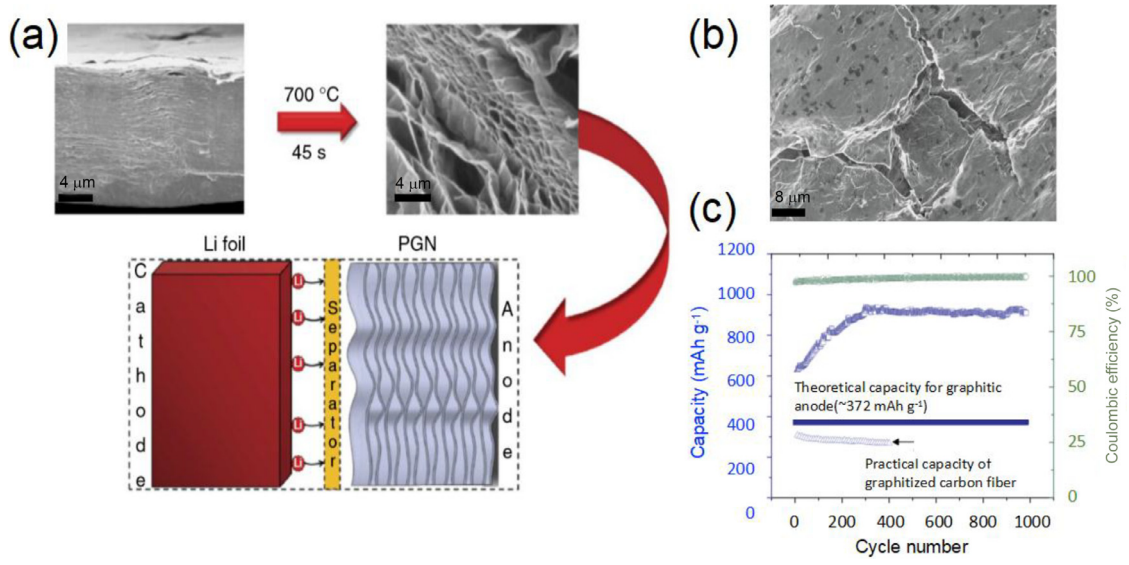

Fig. 7. (a) Synthesis method of a freestanding PGN by thermal shock. (b) SEM image of the lithiated PGN surface showing no visible sharp edges or excessive roughness. The scale bar is 2 μm. (c) Capacity and coulombic efficiency versus cycle index of the PGN anode. Reprinted with permission from Ref. [96]. Copyright (2014) Published by Macmillan Publishers Limited.

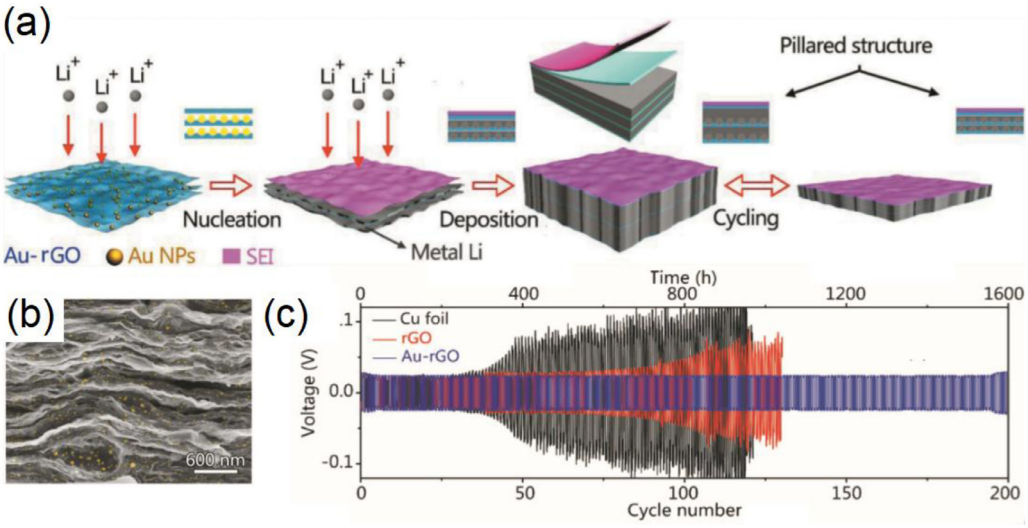

Fig. 8. (a) Schematic of Li deposition on the gold nanoparticles pillared rGO. (b) SEM image of Au-rGO. (c) Voltage–time profiles of lithium plating/stripping cycles at 0.5 mA cm^{-2}. Reprinted with permission from Ref. [77]. Copyright (2018) Published by WILEY-VCH Verlag GmbH & Co. KGaA, Weinheim.

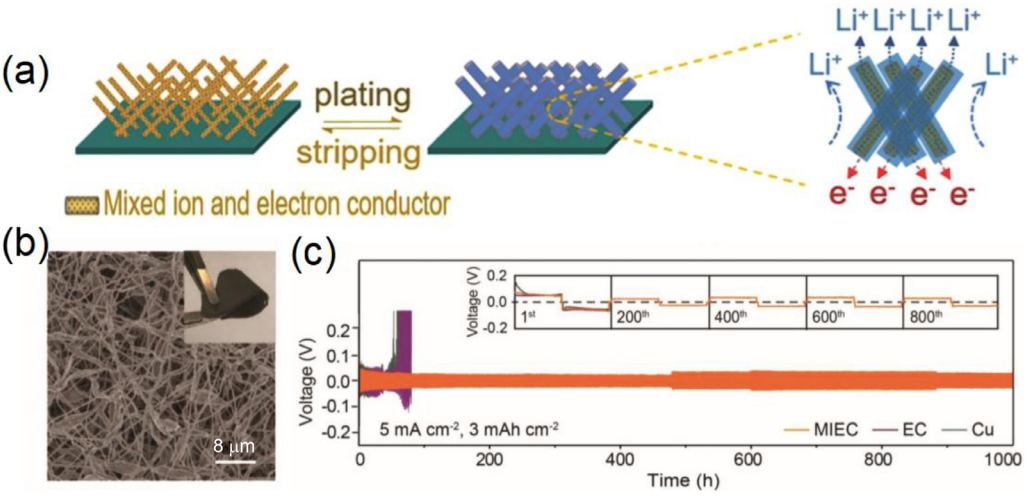

Fig. 9. (a) Schematic of Li plating/stripping behaviors on mixed ion and electron conductor. (b) SEM image of MIEC. Inset: Photograph showing the flexibility of the MIEC membrane. (c) Galvanostatic cycling of symmetric Li/MIEC–Li, Li/EC–Li, and Li/Cu–Li cells at 5 mA cm^{-2}. Reprinted with permission from Ref. [79]. Copyright (2018) Published by WILEY-VCH Verlag GmbH & Co. KGaA, Weinheim.

as seeds to guide the lithium nucleation and following deposition owing to a lower nucleation energy barrier. Braun's group designed a gold nanoparticles pillared rGO composite anode (Fig. 8a) [77]. In this structure, rGO has a high nucleation energy barrier and gold has a low barrier to Li plating. Therefore, rGO was exposed at the electrode surface and gold was placed between the rGO sheets to induce lithium deposition (Fig. 8b). The sandwich structure suppressed lithium dendrite growth because the lithium deposition was guided by the nucleation process instead of electric fields or Li-ion concentration. As a result, the Au-rGO/Li electrode demonstrated a capacity of 2 mAh cm^{-2} for 1600 h and coulombic efficiency up to 98% for 200 cycles (Fig. 8c), which is outstanding among the lithium metal anodes. Tour's group also reported a graphene–carbon nanotube (GCNT) electrode with a Cu substrate [78]. The GCNT was grown on a Cu substrate via chemical vapor deposition, followed by the deposition of iron nanoparticles and aluminum oxide on top. The average electronic conductivity of this electrode is 1.45×10^3 S m^{-1} from the Cu current collector to the GCNT. Combining the features of high conductivity, high porosity, high surface area, and low mass density, Li deposition could be regulated on the surface of the CNT structure. It was observed that instead of plating on top as a film, Li was plated inside the CNT structure homogeneously. As a result, GCNT demonstrated a small polarization of 100 mV at 0.7 mAh cm^{-2} and a capacity of 3351 mAh $g_{GCNT\text{-}Li}{}^{-1}$ at 4 mAh cm^{-2}. More composite frameworks were designed in this way, such as a 3D graphene coated Ni scaffold [98], which made use of the strong surface-coated graphene layer and the porous metal structure to suppress dendrite growth.

A lithium compound is a Li^+ ion conductor that can offer sufficient Li^+ ions and regulate Li^+ ion distribution. By combining the lithium compound and carbon-based framework, an ion and electron bi-continuous conducting mechanism was proposed [99–102]. Luo's group designed a mixed scaffold that put $Li_{6.4}La_3Zr_2Al_{0.2}O_{12}$ (LLZO) nanoparticles into 3D CNFs (Fig. 9a, b) [79]. They mentioned that in an electron-conducting (EC) matrix, the insufficient Li/electrolyte interface restrained the rate performance of the electron-conducting matrix [103]. Therefore, they introduced LLZO nanoparticles into CNFs as a mixed ion and electron conducting scaffold (MIEC) to enhance the CNFs' surface roughness and decrease the interface energy between the CNFs and liquid electrolyte, thus improving the electrolyte wettability of CNFs. Moreover, the homogenously distributed LLZO nanoparticles guided

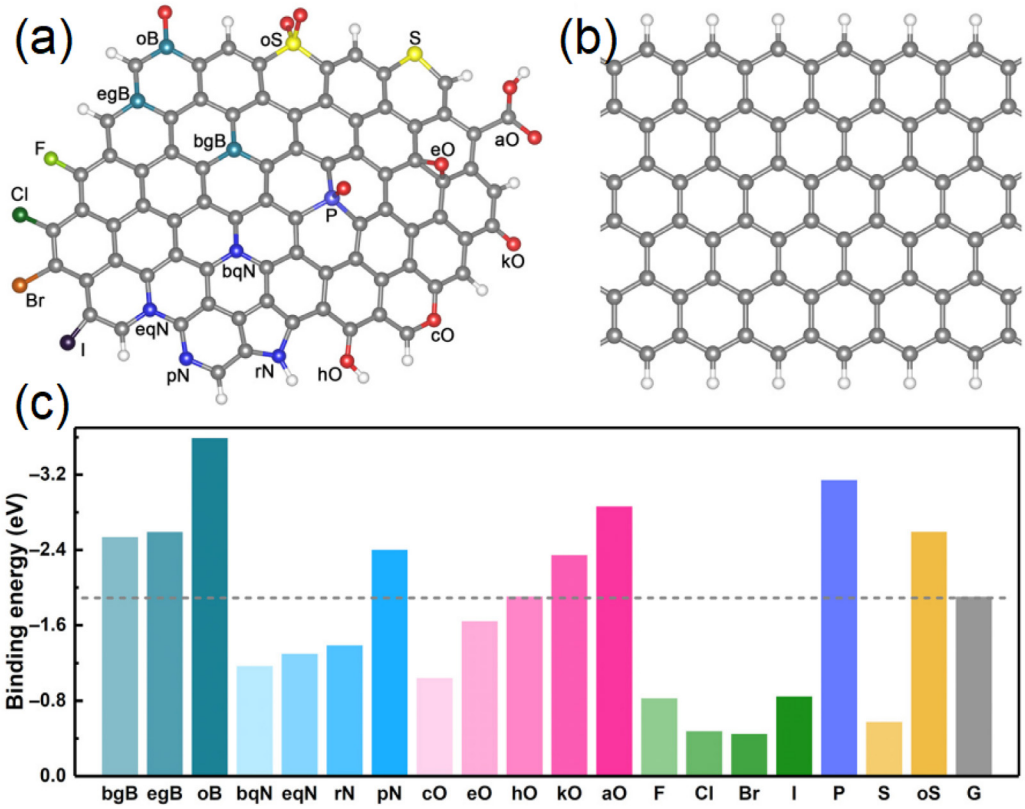

Fig. 10. Modeling of (a) heteroatom-doped carbons and (b) pristine graphene nanoribbons. (c) Calculations of binding energy between heteroatom-doped carbon and a Li atom, including graphitic boron in the bulk phase (bgB), graphitic boron on the edge (egB), B–2C–O–type boron (oB), quaternary nitrogen in the bulk phase (bqN), quaternary nitrogen on the edge (eqN), pyrrolic nitrogen (rN), pyridinic nitrogen (pN), carboxylic group (aO), cyclic oxygen (cO), epoxy group (eO), hydroxyl group (hO), ketone group (kO), and sulfonyl group (oS). Reprinted with permission from Ref. [113]. Copyright (2017) Published by 2019 American Association for the Advancement of Science.

Li^+ ion to distribute evenly and compensated part of the Li^+ ions reduction near the electrode surface by its low ion conductivity. These features led to homogenous Li plating on carbon nanofibers, which resulted in stable cycling over 1000 h at 5 mA cm^{-2} (Fig. 9c).

Mixing ion and electronic paths may be a promising design to obtain high energy density, high power density, and long lifespan [104]. The conductive host is required to accommodate Li deposition, transfer of electrons, and suppression of dendrite growth, whereas ion transport is also crucial to maintain a stable metallic Li morphology at the interface with the electrolyte, especially at a high current density. However, the mixing frameworks require a complex process and expensive price, thus a hybrid framework that is simple and effective in design may be more supportive for practical applications.

4. Lithiophilic 3D framework

As low Li^+ ion concentration and localization of current density promotes dendrite growth, the Li deposition morphology is affected by the Li^+ ionic mass transfer rate to the electrode surface. The lithium ion from electrolyte cannot satisfy the requirement to form uniform crystal nucleus as the reaction proceeds, which would make the lithium ions to deposit on several sites rather than on the whole structure, and then the dendrites are formed [105–109]. Conductive nanostructure boasts high conductivity and specific surface area, which can decrease the current density and form a uniform electric field distribution. However, the traditional conductive structures can hardly adjust the concentration of lithium ions in the electrolyte and electrolyte/Li interface due to the poor Li^+ ions absorbing ability.

The needs for improved adsorption of materials and wetting capacities of lithium become more and more urgent nowadays. Inspired by the hydrophilic porous framework, Cui and co-workers put forward a new concept, “lithiophilicity,” based on previous studies related to the wetting behavior of lithium [110]. “Lithiophilicity” is the wetting property between the molten lithium and network surface, which is described by contact angle and infiltration rate. The binding energy and the Gibbs free energy of a reaction between the materials and lithium can assess their lithiophilicity by first-principle and density functional theory (DFT) calculations [111]. Several methods, listed below, are able to promote lithium ion nucleation early and even guide the crystal nucleus distribution, thereby inhibiting the formation of lithium dendrites and optimizing the cycling stability:

(1) Connecting the polar functional groups that can absorb lithium ions deposition in the Li/electrolyte interface; (2) introducing active compounds that can react with lithium, such as lithiophilic metals and metal oxides.

4.1. Lithiophilic functional groups contained 3D framework

A typical way to obtain lithiophilicity is to decorate the current collector with uniform lithiophilic functional groups [112–115]. These polar functional groups can absorb lithium ions in the electrolyte and gradually release them. After being released, Li^+ ions will form crystal nuclei uniformly on the current collectors, which therefore shows that the design has prevented the lithium metal from nucleating on the irregular defects. Zhang et al. proposed a nitrogen-doped graphene structure with abundant polar functional groups, including pyrrolic, pyridinic, and quaternary nitrogen atoms. This material realized the lithiophilic collector surface, so

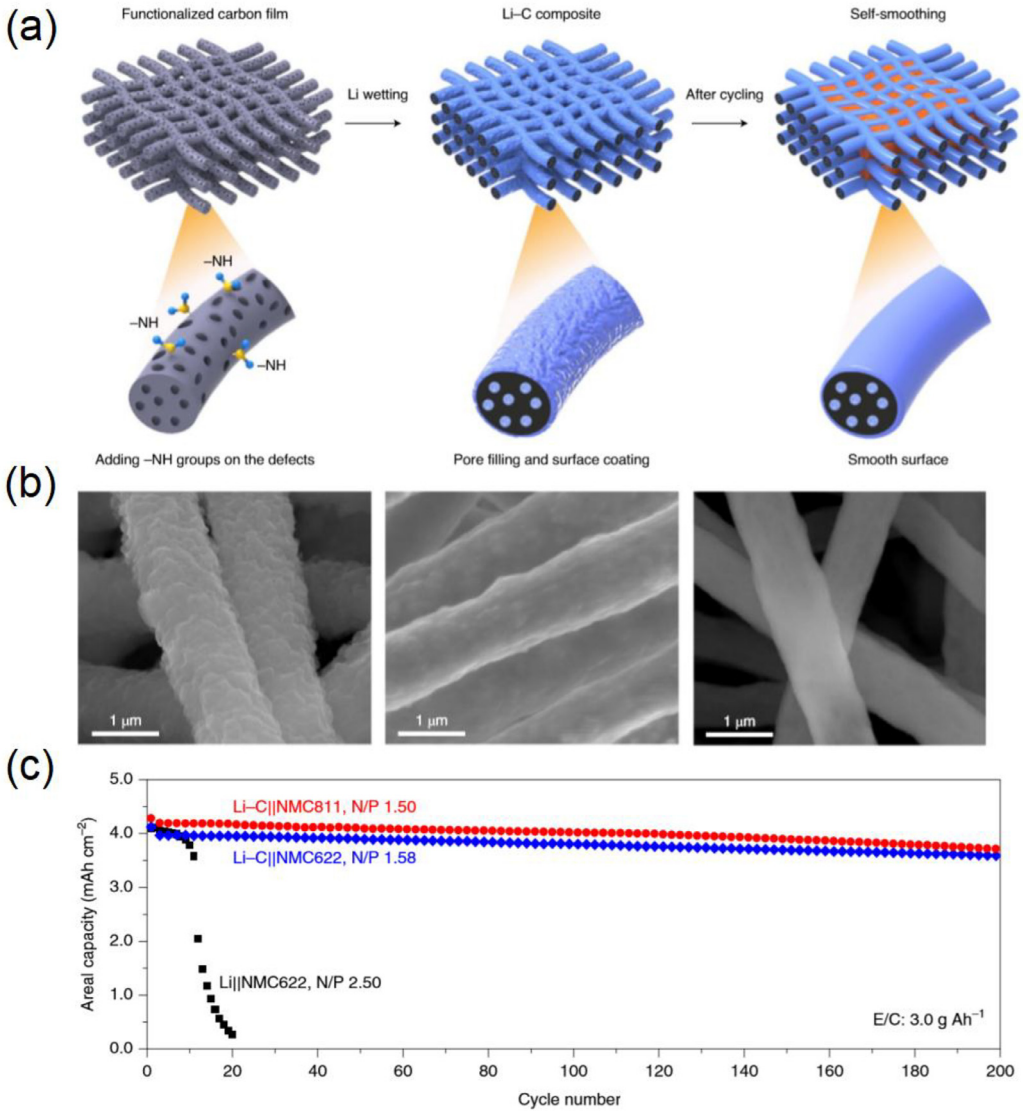

Fig. 11. (a) Schematic of Li/C electrode and its cycling behavior. (b) SEM images of a pristine rough Li–C film before cycling, after 10 cycles and 200 cycles, respectively. (c) Cycling performances of the Li–C||NMC811 ($LiNi_{0.8}Mn_{0.1}Co_{0.1}O_2$), Li–C||NMC622 ($LiNi_{0.6}Mn_{0.2}Co_{0.2}O_2$), and Li||NMC622 cells. Reprinted with permission from Ref. [116]. Copyright (2019) Published by Springer Nature.

lithium ions could nucleate uniformly on the collector during the electrochemical cycles. Binding energy and charge density analyses between the Li atom and polar nitrogen were obtained by DFT calculations. They revealed that pyrrolic nitrogen and pyridinic nitrogen have large binding energies of 4.46 and 4.26 eV and high local charge density with Li atoms, which indicates that Li and N atoms has a strong interaction. Li^+ ions tend to be attracted and plated near these lithiophilic nitrogen functional groups sites as they have stronger binding energy and better adsorption of Li^+ ions. Because of the strategy of inhibiting the lithium ion early nucleation process, a coulombic efficiency of 98% is maintained nearly 200 cycles at 1.0 mA cm^{-2} current density [81]. They also constructed models of graphene nanoribbons (Fig. 10b) and a series of heteroatom-doped carbons (Fig. 10a) to further understand the Li nucleation process. A summary of the binding energy between various atoms and Li atom was then introduced (Fig. 10c), which revealed that graphene nanoribbons with some dopant atoms such as bgB, egB, pN, kO, and aO have larger binding energy than others, which opened the way for other possible frameworks to be explored [113]. Besides, Zhang and his co-workers constructed a 3D glass fiber cloth with polar functional groups as the barrier layer of the lithium electrode to uniformly distribute Li ions [62], which resulted in deposition without dendrites even at 10.0 mA cm^{-2}.

A layered Li–rGO electrode synthesized by infusing molten Li into an rGO film was designed by Lin et al. [60]. In this structure, the layered rGO structure offered large surface area and pore volume to accommodate Li deposition and mitigate the volume change during cycling. The rGO structure also had polar functional groups such as carbonyl and alkoxy groups that exhibited high binding energy to Li. This increased the lithiophilicity to induce Li^+ ion. In addition, the top rGO layer could stabilize the as-formed SEI by its electrochemically and mechanically stable interface. A Li/C anode based on mesoporous carbon nanofibers was presented by Niu et al. (Fig. 11a) [116] by attaching -NH functional groups on the defects of carbon films, and the wettability of Li on the carbon surface was greatly improved. The strong interaction between -NH functional groups and Li metal led to a Li nucleation preferentially in the pores and/or the cavities in a homogenous morphology, which exhibited a reversible and “self-smoothing” Li deposition. It was observed that the rough electrode surface was gradually smoothed out in the early stages, which indicated that Li dendrites were suppressed (Fig. 11b). The assembled

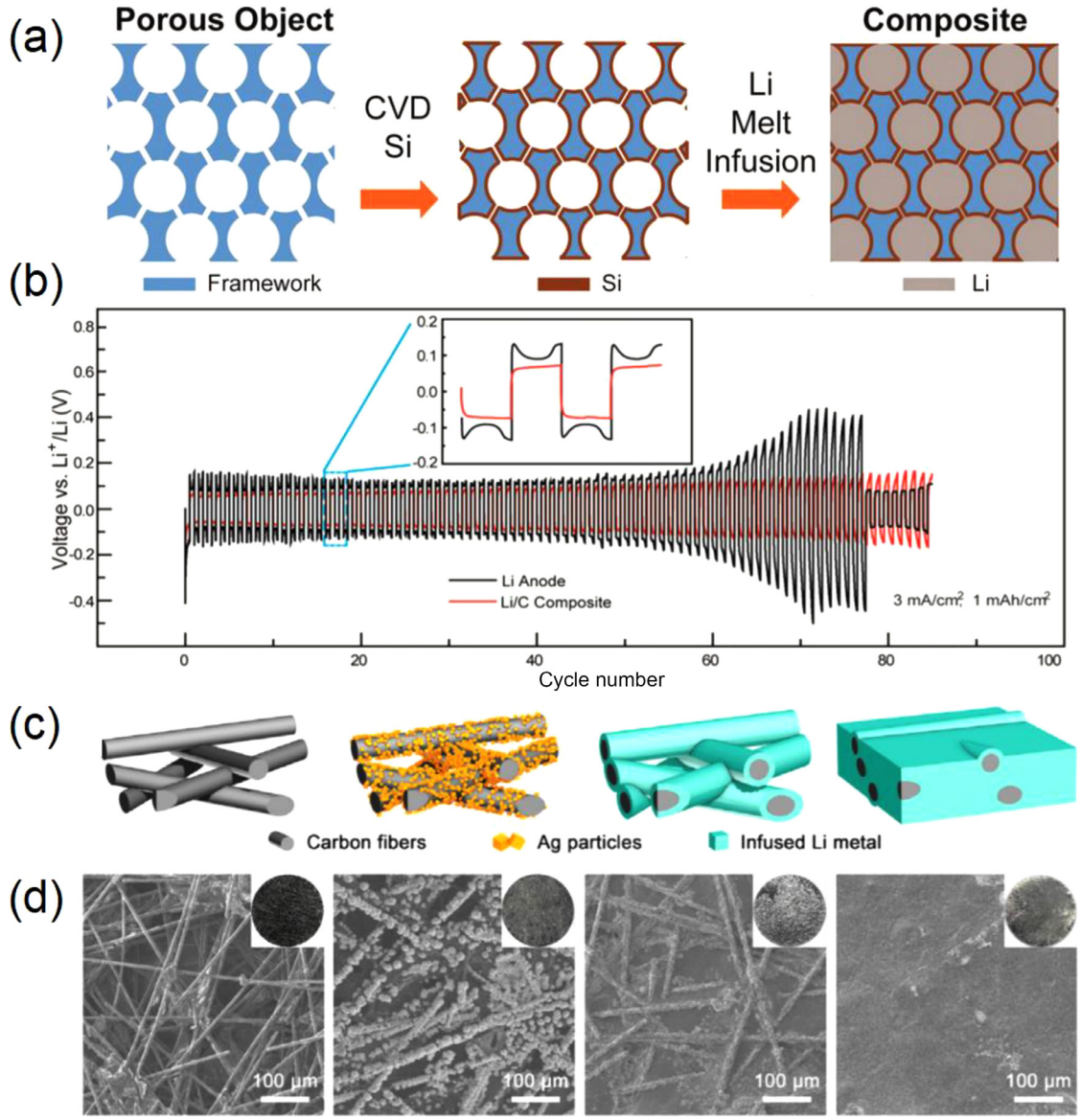

Fig. 12. (a) Schematic of the design of Si/CNF framework. (b) Galvanostatic cycling of Li/C and bare Li symmetrical cells at 3 mA cm^{-2} for a total of 1 mAh cm^{-2}. Reprinted with permission from Ref. [80]. Copyright (2016) Published by National Academy of Sciences. Schematic (c) and SEM images (d) of Ag layer electroplates on pristine CF and molten Li infusion on CF framework. Reprinted with permission from Ref. [121]. Copyright (2018) Published by Elsevier Inc.

Li metal battery, in which the anode was coupled with a lithium nickel–manganese–cobalt oxide cathode with high nickel content (negative/positive electrode capacity ratio of 1.5) and an extremely lean electrolyte (electrolyte amount to cathode capacity ratio of 3 g Ah^{-1}) was used (Fig. 11c), delivered a cell-level energy density of 350–380 Wh kg^{-1} during stable cycling for 200 cycles. Moreover, porphyrin-derived graphene-based nanosheets [82], metal–organic framework [117], MXene aerogel scaffolds [118], polymer nanofiber [119], and pyrolyzed N-doped binder network [120] are also designed to block lithium dendrite growth.

Introducing lithiophilic functional groups is a direct and efficient method to absorb Li atoms, and there are wide options of dopant atoms. For carbon-based lithiophilic frameworks, both the electron conductivity and lithiophilic property not only benefit Li absorption, but also increase the electroactive surface area. However, the introduction of heteroatoms or organics groups would decrease the electron conductivity, and thus, the doped amount needs to be reasonably controlled. For non-conductive lithiophilic frameworks, Li metal tends to plate on the current collector, where Li metal as the sole electron conductor easily loses electric contact.

4.2. Lithiophilic-interlayer-forming 3D framework

Lithium can react with metal, metal oxide, or other substances to form a compound that exhibits significant lithiophilicity. By evenly pouring molten lithium into a CNT/Si matrix, Cui and co-workers constructed a promising stable lithium-scaffold anode (Fig. 12a), which had relatively large surface and chemical stability [80]. They selected Si as the lithiophilic material to improve the lithiophilicity of the porous carbon scaffold prominently. The thin layer of Si was embedded into the carbon fiber matrix with an average diameter of 196 nm, then the intermediate was disposed via chemical vapor deposition, and finally, the nanostructure was obtained. The Li/Si alloy could effectively induce the uniform deposition of lithium ions, reducing the interfacial impedance, and thus avoiding the growth of dendrites. It could deliver a volumetric capacity of approximately 1900 mAh cm^{-3} and little polarization appeared for 80 cycles at 3 mA cm^{-2} (Fig. 12b).

The lithiophilic metal can provide both electron and Li^+ ion control, which makes it an efficient method to suppress dendrite growth. Zhang et al. presented a cheaper and more efficient way to

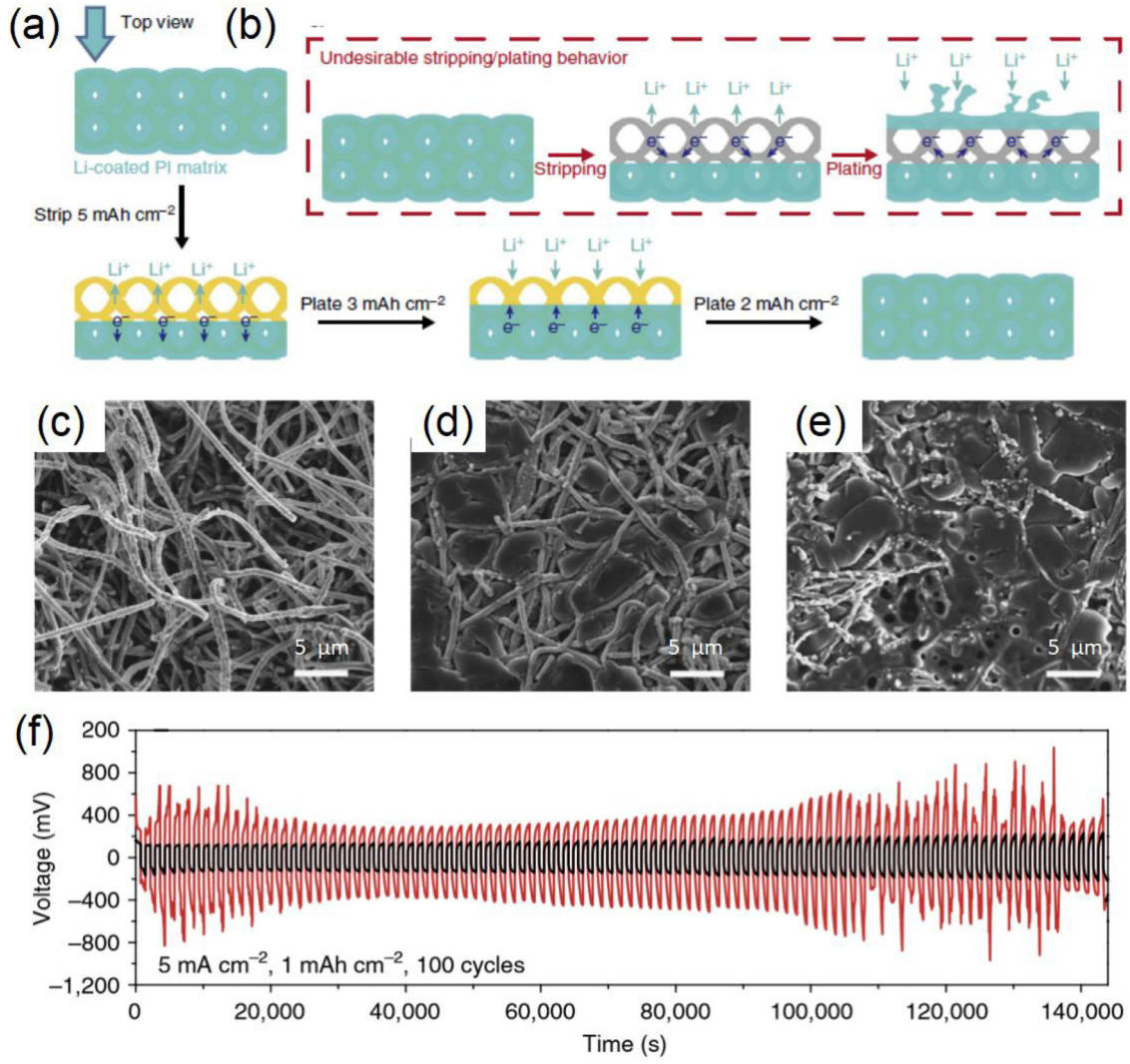

Fig. 13. (a) Schematic of the Li stripping/plating on Li-coated PI/ZnO matrix. (b) Undesirable Li stripping/plating on carbon framework. Top-view, SEM images of the exposed top fibers of the Li-coated PI electrode after stripping away 5 mAh cm^{-2} Li (c), plating 3 mAh cm^{-2} Li back (d), and completely filled with Li (e). (f) Galvanostatic cycling of the Li-coated PI matrix and the bare Li electrode at 5 mA cm^{-2}. Reprinted with permission from Ref. [58]. Copyright (2016) Published by Nature Publishing Group.

electroplate a lithiophilic silver layer onto a coralloid fiber for the formation of a Li electrode (Fig. 12c,d) [121]. The CF/Ag framework could be fully infused by molten Li in 1–3 min and form a Li/Ag alloy interlayer. The Li/Ag alloy interlayer could not only improve the wetting ability for the coralloid fiber skeleton to siphon the molten lithium, but also reduce the lithium's deposition overpotential owing to its outstanding lithiophilicity. The composite anode showed excellent cycling stability without dead lithium. It could achieve 64.3% capacity retention for 400 cycles at 0.5 °C and showed small dendrite growth even at 10.0 mA cm^{-2}. As shown by the properties of the silver layer, many transition metals like Ge [122] and Sn [123] can also react with molten lithium to form Li/Ge and Li/Sn alloys. It is also feasible to directly introduce an alloy layer that owns excellent lithiophilicity [124,125].

Aside from alloy reactions, conversion reactions between Li and some metal oxides can also be carried out to produce a lithiophilic interlayer. Cui and co-workers reported a core-shell polyimide matrix coated with a conformal ZnO layer (Fig. 13a) [58]. In conventional frameworks, Li integrates with electrons and Li^+ ions on the surface and nucleates on the top surface directly, leaving the internal structure empty (Fig. 13b). In this structure, the electrospun polymeric fibers formed a chemically and electrochemically inert matrix, which could efficiently regulate the Li deposition progress. The ZnO layer could react with the molten lithium and showed great lithiophilicity. It could be observed that the top Li layers were dissolved during stripping and plated back with no obvious dendrite (Fig. 13c-e). This Li-coated PI anode showed stable cycling, for more than 100 cycles at 5 mA cm^{-2} (Fig. 13f). As a typical lithiophilic material, ZnO has also been used to modify other Li host materials, such as highly porous carbonized wood, hierarchical carbon scaffold, and Cu foam, to improve the frameworks' lithiophilicity [126–129]. Besides, Chen et al. demonstrated a series of other transition metal oxides such as MnO_2, Co_3O_4, and SnO_2 nanoflake arrays, all of which are strong oxidizing agents and can react with molten lithium [130]. The metal oxide nanoflakes decorated the surface of graphene foams (GFs) and the melt Li infusion process was efficiently achieved, which ensured excellent lithiophlicity and strong bonding to the Li metal. MnO_2 (or other transition metal oxide) and the containing solid H_2O could react with the infusing Li to form a strong bonding between the surface of nanoflakes and molten Li as the following chemical Eqs. (3) and (4):

$$2\ Li + 2\ H_2O \rightarrow 2\ LiOH + H_2\uparrow \quad (3)$$

$$MnO_2 + 4\ Li \rightarrow Mn + 2\ Li_2O_2 \quad (4)$$

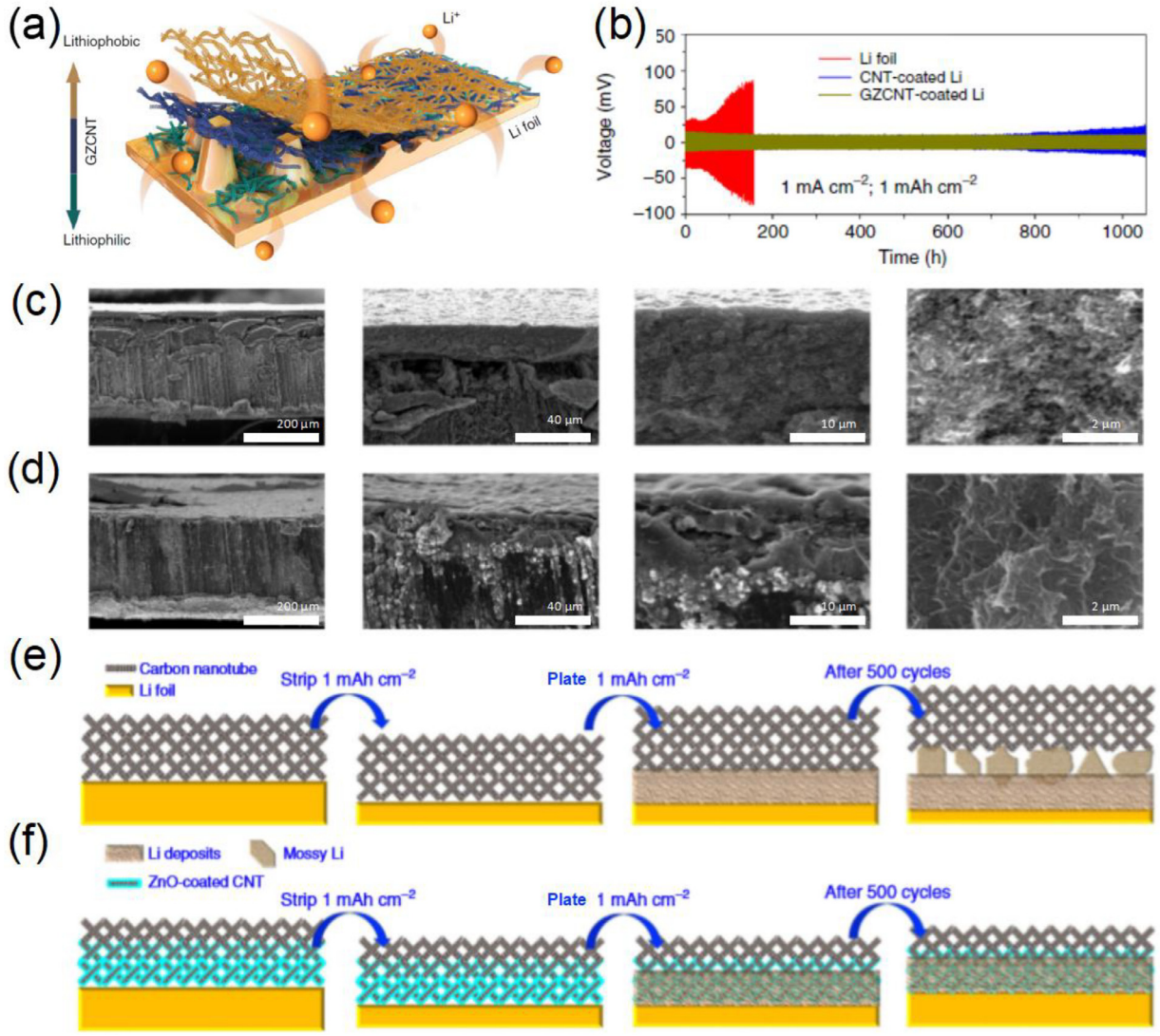

Fig. 14. (a) Schematic of synthesis of the interfacial layer in a glove box. (b) Comparison of the cycle ability and polarization of a symmetric cell. SEM images of the Li cells coated with a CNT (c) or GZCNT (d) interfacial layer with various magnifications at a current density of 1 mA cm^{-2} after 520 cycles. Li stripping mechanism of CNT-coated Li foils (e) and GZCNT interfacial layer (f). Reprinted with permission from Ref. [83]. Copyright (2018) Published by Nature Publishing Group.

The resulting composite anode based on 3D graphene foam shows great affinity with molten Li and favorable cycling stability for Li dissolution–precipitation. Other lithiophilic oxides work in the same way [131–133].

The lithiophilic interlayer formed by the conversion or alloy reactions of the composite electrode exhibits good Li absorptivity. However, the thickness of the interlayer and consumption of Li^+ ion are still difficult to be quantized, owing to an uncontrollable infiltration of the molten lithium. Thus, the construction of the specific lithiophilic composite frameworks with a controlled interlayer needs to be considered to achieve both high absorption ability and less Li consumption.

4.3. Lithiophilic–lithiophobic gradient 3D framework

By making use of the lithiophilic/lithiophobic materials and arranging them carefully, it is possible to regulate the Li deposition more efficiently [134–136]. Pu et al. proposed a “top-growth” mode where Li deposition preferentially began from the anode/separator interfaces, which would cause direct dendrite growth and penetrate the separator [137]. To suppress this top-growth mode, it is viable to induce Li deposition at the bottom. Zhang et al. have applied lithiophilic ZnO and lithiophobic carbon nanotube to design a lithiophilic–lithiophobic gradient framework (GZCNT), which restrained dendrite growth and improved the cycle property in the current collector successfully (Fig. 14a) [83]. It was composed of three parts including the lithiophilic bottom, intermediate transition layer, and lithiophobic top. The bottom is a composite of zinc oxide and carbon nanotube sublayer, and the ZnO particles remarkably decentralize on a single carbon nanotube. An interesting phenomenon is that the lithiophilic bottom structure adheres to the lithium foil tightly, which facilitates a uniform lithium diffusion and establishes a stable solid electrolyte interphase at the same time. The middle buffer layer could prevent a lithium dendrite graded layer as the result of sudden transformation between lithiophilic and lithiophobic. The top part is a lithiophobic carbon nanotube sublayer whose binding energy with Li is even low, approximately 1.19 eV. Its large area with porous structure gives it an ability to prevent further growth of lithium dendrites effectively. In CNT-coated frameworks, mossy Li grew in the voids, which would consume the electrolyte to exhaustion and result in the failure of the cell (Fig. 14c,e). On the contrary, GZCNT’s top lithiophobic layer offered a large surface area where Li could diffuse and deposit in the interspace without dendrite formation, whereas the bottom

lithiophilic layer effectively facilitated a homogenous Li deposition morphology. As a result, there was no formation of dendrites or corrosion layer between the CNT and Li foil (Fig. 14d,f). The whole structure with this well-designed layer could block dendrite growth and regulate the lithium dissolution/deposition process during charge–discharge cycles, obtaining the best stability of 520 cycles with a low overpotential of 25 mV at 1 mA cm^{-2} (Fig. 14b).

5. Conclusions and outlooks

In conclusion, we discussed three dimensional porous frameworks for suppressing lithium dendrite in terms of conductive 3D frameworks and lithiophilic 3D framework. Conductive 3D frameworks make use of its high electroactive surface area to reduce the current density and homogenize the electric field of the Li deposition site, thereby regulating the Li plating morphology. Carbon-based frameworks have high conductivity, light weight, and facile preparation, bringing in multiple possible nanostructures and various applications in the battery. Metal-based frameworks have better mechanical strength and conductive continuity, offering high active surface area and Li metal regulation; prior studies on these frameworks mainly focus on the modification and pore construction in current collectors. Lithiophilic frameworks focus on using lithiophilic functional groups or active compounds to better adsorb Li^+ ion, adjust the concentration of Li^+ ion in the electrolyte and electrolyte/Li interface, further inducing Li^+ ion to deposit homogeneously. An effective method of pouring molten lithium into the frameworks is proposed and widely applied.

Although some improvements on Li host frameworks have been achieved, and the composited 3D Li anodes have also exhibited low polarization and long cycle life in the laboratory, numerous challenges still need to be overcome to achieve a commercialization-level Li metal anode for high-specific-energy and safe Li metal cells. These mainly include the amount of introduced frameworks and lithium and their massive manufacture. (1) The 3D frameworks would introduce a mass of voids and additional inactive weight in the anode; thus, the porosity, surface area, and amount of Li loading should be precisely controlled for practical applications. The mass ratio of Li to host materials should be maximized. (2) The commercial Li metal batteries need very thin Li anodes and the Li-plating/stripping-caused volume change is drastic. Therefore, high electron conduction, lithiophilic ability, and high strength of the host framework are all required. (3) The available 3D frameworks could be mass-produced and at low cost. (4) The available 3D frameworks must be easily processable, scalable, and compatible for particle cell manufacturing. (5) The large surface area of the 3D frameworks would trigger abundant side reactions with the electrolyte, which requires a more stable 3D framework, electrolyte composition, and SEI design.

Besides, the safety and reliability of the commercial Li metal batteries applied for electric vehicles and other electrical applications still require numerous tests. Meanwhile, the recoverability of expensive Li metal batteries should also be considered as an important issue to be solved for continued energy storage. We hope that this review will provide significant enlightenment and reference for the future researches on Li metal batteries.

Declaration of Competing Interests

The authors declare no competing financial interests.

Acknowledgments

This work was supported by the National Natural Science Foundation of China (51521001, 51832004 and 51602239), the National Natural Science Fund for Distinguished Young Scholars (51425204), and the Programme of Introducing Talents of Discipline to Universities (B17034), the Yellow Crane Talent (Science & Technology) Program of Wuhan City.

Supplementary materials

Supplementary material associated with this article can be found, in the online version, at doi:10.1016/j.jechem.2019.09.031.

References

[1] E.C. Evarts, Nature 526 (2015) S93–S95.
[2] L. Grande, E. Paillard, J. Hassoun, J.B. Park, Y.J. Lee, Y.K. Sun, S. Passerini, B. Scrosati, Adv. Mater. 27 (2015) 784–800.
[3] J.M. Tarascon, M. Armand, Nature 414 (2001) 359–367.
[4] W. Xu, J.L. Wang, F. Ding, X.L. Chen, E. Nasybutin, Y.H. Zhang, J.G. Zhang, Energ. Environ. Sci. 7 (2014) 513–537.
[5] X.L. Ji, K.T. Lee, L.F. Nazar, Nat. Mater. 8 (2009) 500–506.
[6] H.L. Wang, Y. Yang, Y.Y. Liang, J.T. Robinson, Y.G. Li, A. Jackson, Y. Cui, H.J. Dai, Nano Lett. 11 (2011) 2644–2647.
[7] P.G. Bruce, S.A. Freunberger, L.J. Hardwick, J.M. Tarascon, Nat. Mater. 11.1 (2012) 19.
[8] J. Xiao, D.H. Mei, X.L. Li, W. Xu, D.Y. Wang, G.L. Graff, W.D. Bennett, Z.M. Nie, L.V. Saraf, I.A. Aksay, J. Liu, J.G. Zhang, Nano Lett. 11 (2011) 5071–5078.
[9] C.Z. Yuan, H.B. Wu, Y. Xie, X.W. Lou, Angew. Chem. Int. Edit. 53 (2014) 1488–1504.
[10] Y.C. Lu, Z.C. Xu, H.A. Gasteiger, S. Chen, K. Hamad-Schifferli, Y. Shao-Horn, J. Am. Chem. Soc. 132 (2010) 12170–12171.
[11] L. Gireaud, S. Grugeon, S. Laruelle, B. Yrieix, J.M. Tarascon, Electrochem. Commun. 8 (2006) 1639–1649.
[12] J.L. Barton, J.O. Bockris, Proc. Royal Soc. Lond. A. Math. Phys. Sci. 268 (1962) 485–505.
[13] R. Akolkar, J. Power Sources 246 (2014) 84–89.
[14] M. Dolle, L. Sannier, B. Beaudoin, M. Trentin, J.M. Tarascon, Electrochem. Solid St. 5 (2002) A286–A289.
[15] J. Steiger, D. Kramer, R. Monig, J. Power Sources 261 (2014) 112–119.
[16] Q.Q. Liu, C.Y. Du, B. Shen, P.J. Zuo, X.Q. Cheng, Y.L. Ma, G.P. Yin, Y.Z. Gao, Rsc. Adv. 6 (2016) 88683–88700.
[17] M. Winter, B. Barnett, K. Xu, Chem. Rev. 118 (2018) 11433–11456.
[18] X.-Q. Zhang, C.-Z. Zhao, J.-Q. Huang, Q. Zhang, Engineering 4 (2018) 831–847.
[19] X.-B. Cheng, C.-Z. Zhao, Y.-X. Yao, H. Liu, Q. Zhang, Chem. 5 (2019) 74–96.
[20] X. Xu, S. Wang, H. Wang, C. Hu, Y. Jin, J. Liu, H. Yan, J. Energy Chem. 27 (2018) 513–527.
[21] J. Cui, T.-G. Zhan, K.-D. Zhang, D. Chen, Chin. Chem. Lett. 28 (2017) 2171–2179.
[22] H. Kuwata, H. Sonoki, M. Matsui, Y. Matsuda, N. Imanishi, Electrochem. 84 (2016) 854–860.
[23] J. Heine, P. Hilbig, X. Qi, P. Niehoff, M. Winter, P. Bieker, J. Electrochem. Soc. 162 (2015) A1094–A1101.
[24] J. Guo, Z.Y. Wen, M.F. Wu, J. Jin, Y. Liu, Electrochem. Commun. 51 (2015) 59–63.
[25] H. Sano, H. Sakaebe, H. Matsumoto, J. Power Sources 196 (2011) 6663–6669.
[26] R. Murugan, V. Thangadurai, W. Weppner, Angew. Chem. Int. Edit. 46 (2007) 7778–7781.
[27] X.F. Yan, Z.B. Li, Z.Y. Wen, W.Q. Han, J. Phys. Chem. C 121 (2017) 1431–1435.
[28] C. Luo, X. Ji, J. Chen, K.J. Gaskell, X. He, Y. Liang, J. Jiang, C. Wang, Angew. Chem. Int. Edit. 57 (2018) 8567–8571.
[29] Y. Shen, Y. Zhang, S. Han, J. Wang, Z. Peng, L. Chen, Joule 2 (2018) 1674–1689.
[30] N.W. Li, Y.X. Yin, C.P. Yang, Y.G. Guo, Adv. Mater. 28 (2016) 1853–1858.
[31] Y.Y. Liu, D.C. Lin, P.Y. Yuen, K. Liu, J. Xie, R.H. Dauskardt, Y. Cui, Adv. Mater. 29 (2017).
[32] A. Basile, A.I. Bhatt, A.P. O'Mullane, Nat. Commun. 7 (2016) 11794.
[33] Z. Peng, S.W. Wang, J.J. Zhou, Y. Jin, Y. Liu, Y.P. Qin, C. Shen, W.Q. Han, D.Y. Wang, J. Mater. Chem. A 4 (2016) 2427–2432.
[34] H.K. Jing, L.L. Kong, S. Liu, G.R. Li, X.P. Gao, J. Mater. Chem. A 3 (2015) 12213–12219.
[35] C. Yan, X.-B. Cheng, Y.-X. Yao, X. Shen, B.-Q. Li, W.-J. Li, R. Zhang, J.-Q. Huang, H. Li, Q. Zhang, Adv. Mater. 30 (2018) 1804461.
[36] C. Yan, X.-B. Cheng, Y. Tian, X. Chen, X.-Q. Zhang, W.-J. Li, J.-Q. Huang, Q. Zhang, Adv. Mater. 30 (2018) 1707629.
[37] J. Zheng, G. Ji, X. Fan, J. Chen, Q. Li, H. Wang, Y. Yang, K.C. DeMella, S.R. Raghavan, C. Wang, Adv. Energy Mater. 9 (2019) 1803774.
[38] X.-Q. Zhang, X. Chen, X.-B. Cheng, B.-Q. Li, X. Shen, C. Yan, J.-Q. Huang, Q. Zhang, Angew. Chem. Int. Edit. 57 (2018) 5301–5305.
[39] X. Fan, L. Chen, O. Borodin, X. Ji, J. Chen, S. Hou, T. Deng, J. Zheng, C. Yang, S.-C. Liou, K. Amine, K. Xu, C. Wang, Nat. Nanotechnol. 13 (2018) 715–722.
[40] X.-Q. Zhang, X. Chen, L.-P. Hou, B.-Q. Li, X.-B. Cheng, J.-Q. Huang, Q. Zhang, ACS Energy Lett. 4 (2019) 411–416.
[41] X.-B. Cheng, C. Yan, X. Chen, C. Guan, J.-Q. Huang, H.-J. Peng, R. Zhang, S.-T. Yang, Q. Zhang, Chem. 2 (2017) 258–270.
[42] C.-Z. Zhao, X.-B. Cheng, R. Zhang, H.-J. Peng, J.-Q. Huang, R. Ran, Z.-H. Huang, F. Wei, Q. Zhang, Energy Storage Mater. 3 (2016) 77–84.

[43] C. Yan, X.-B. Cheng, C.-Z. Zhao, J.-Q. Huang, S.-T. Yang, Q. Zhang, J. Power Sources 327 (2016) 212–220.
[44] X.-B. Cheng, C. Yan, H.-J. Peng, J.-Q. Huang, S.-T. Yang, Q. Zhang, Energy Storage Mater. 10 (2018) 199–205.
[45] H. Chen, A. Pei, D. Lin, J. Xie, A. Yang, J. Xu, K. Lin, J. Wang, H. Wang, F. Shi, D. Boyle, Y. Cui, Adv. Energy Mater. 0 (2019) 1900858.
[46] W. Deng, W.H. Zhu, X.F. Zhou, Z.P. Liu, Energy Storage Mater. 15 (2018) 266–273.
[47] Y. Zhang, C.W. Wang, G. Pastel, Y.D. Kuang, H. Xie, Y.J. Li, B.Y. Liu, W. Luo, C.J. Chen, L.B. Hu, Adv. Energy Mater. 8 (2018) 1800635.
[48] H.J. Zhao, N.P. Deng, J. Yan, W.M. Kang, J.G. Ju, Y.L. Ruan, X.Q. Wang, X.P. Zhuang, Q.X. Li, B.W. Cheng, Chem. Eng. J. 347 (2018) 343–365.
[49] H. Zhang, C.M. Li, M. Piszcz, E. Coya, T. Rojo, L.M. Rodriguez-Martinez, M. Armand, Z.B. Zhou, Chem. Soc. Rev. 46 (2017) 797–815.
[50] S.Y. Wei, S. Choudhury, J. Xu, P. Nath, Z.Y. Tu, L.A. Archer, Adv. Mater. 29 (2017) 1605512.
[51] S.J.M.D. Zhang, C.C. Chan, Y. Zhou, Energy Storage Sci. Technol. 7 (2018) 646–653.
[52] X.P. Ai, Energy Storage Sci. Technol. 7 (2018) 37–39.
[53] G.Y. Zheng, S.W. Lee, Z. Liang, H.W. Lee, K. Yan, H.B. Yao, H.T. Wang, W.Y. Li, S. Chu, Y. Cui, Nat. Nanotechnol. 9 (2014) 618–623.
[54] S. Sim, P. Oh, S. Park, J. Cho, Adv. Mater. 25 (2013) 4498–4503.
[55] B. Wang, X.L. Li, X.F. Zhang, B. Luo, Y.B. Zhang, L.J. Zhi, Adv. Mater. 25 (2013) 3560–3565.
[56] P. Simon, Y. Gogotsi, B. Dunn, Science 343 (2014) 1210–1211.
[57] X. Zhang, W. Shyy, A.M. Sastry, J. Electrochem. Soc. 154 (2007) S21 S21.
[58] Y. Liu, D. Lin, Z. Liang, J. Zhao, K. Yan, Y. Cui, Nat. Commun. 7 (2016) 10992.
[59] S. Liu, X. Xia, Y. Zhong, S. Deng, Z. Yao, L. Zhang, X.-B. Cheng, X. Wang, Q. Zhang, J. Tu, Adv. Energy Mater. 8 (2018) 1702322.
[60] D. Lin, Y. Liu, Z. Liang, H.W. Lee, J. Sun, H. Wang, K. Yan, J. Xie, Y. Cui, Nat. Nanotechnol. 11 (2016) 626–632.
[61] A. Wang, X. Zhang, Y.-W. Yang, J. Huang, X. Liu, J. Luo, Chem. 4 (2018) 2192–2200.
[62] X.B. Cheng, T.Z. Hou, R. Zhang, H.J. Peng, C.Z. Zhao, J.Q. Huang, Q. Zhang, Adv. Mater. 28 (2016) 2888–2895.
[63] P. Shi, T. Li, R. Zhang, X. Shen, X.-B. Cheng, R. Xu, J.-Q. Huang, X.-R. Chen, H. Liu, Q. Zhang, Adv. Mater. 31 (2019) 1807131.
[64] X. Shen, X. Cheng, P. Shi, J. Huang, X. Zhang, C. Yan, T. Li, Q. Zhang, J. Energy Chem. 37 (2019) 29–34.
[65] D. Wang, C. Luan, W. Zhang, X. Liu, L. Sun, Q. Liang, T. Qin, Z. Zhao, Y. Zhou, P. Wang, W. Zheng, Adv. Energy Mater. 8 (2018) 1800650.
[66] L.L. Lu, J. Ge, J.N. Yang, S.M. Chen, H.B. Yao, F. Zhou, S.H. Yu, Nano Lett. 16 (2016) 4431–4437.
[67] X. Ke, Y.F. Cheng, J. Liu, L.Y. Liu, N.G. Wang, J.P. Liu, C.Y. Zhi, Z.C. Shi, Z.P. Guo, ACS Appl. Mater. Inter. 10 (2018) 13552–13561.
[68] C.P. Yang, Y.X. Yin, S.F. Zhang, N.W. Li, Y.G. Guo, Nat. Commun. 6 (2015) 8058.
[69] Q.B. Yun, Y.B. He, W. Lv, Y. Zhao, B.H. Li, F.Y. Kang, Q.H. Yang, Adv. Mater. 28 (2016) 6932.
[70] S.-H. Wang, Yin, Y.-X. Zuo, T.-T. Dong, W. Li, J.-Y. Shi, J.-L. Zhang, C.-H. Li, N.-W. Li, C.-J. Guo, Y.-G, Adv. Mater. 29 (2017) 1703729.
[71] P.C. Zou, Y. Wang, S.W. Chiang, X.Y. Wang, F.Y. Kang, C. Yang, Nat. Commun. 9 (2018) 464.
[72] H. Lee, J. Song, Y.J. Kim, J.K. Park, H.T. Kim, Sci. Rep. 6 (2016) 30830.
[73] A.Y. Zhang, X. Fang, C.F. Shen, Y.H. Liu, C.W. Zhou, Nano Res. 9 (2016) 3428–3436.
[74] T.T. Zuo, X.W. Wu, C.P. Yang, Y.X. Yin, H. Ye, N.W. Li, Y.G. Guo, Adv. Mater. 29 (2017) 1700389.
[75] J.W. Xiang, Y. Zhao, L.X. Yuan, C.J. Chen, Y. Shen, F. Hu, Z.X. Hao, J. Liu, B.X. Xu, Y.H. Huang, Nano Energy 42 (2017) 262–268.
[76] Z.H. Wang, X.D. Wang, W. Sun, K.N. Sun, Electrochim. Acta. 252 (2017) 127–137.
[77] J. Pu, J.C. Li, Z.H. Shen, C.L. Zhong, J.Y. Liu, H.X. Ma, J. Zhu, H.G. Zhang, P.V. Braun, Adv. Funct. Mater. 28 (2018) 1804133.
[78] A.R.O. Raji, R.V. Salvatierra, N.D. Kim, X.J. Fan, Y.L. Li, G.A.L. Silva, J.W. Sha, J.M. Tour, ACS Nano 11 (2017) 6362–6369.
[79] C.Y. Zhang, S. Liu, G.J. Li, C.J. Zhang, X.J. Liu, J.Y. Luo, Adv. Mater. 30 (2018) 1801328.
[80] R. Zhang, X.R. Chen, X. Chen, X.B. Cheng, X.Q. Zhang, C. Yan, Q. Zhang, Angew. Chem. Int. Ed. Engl. 56 (2017) 7764–7768.
[81] L. Kong, B.-Q. Li, H.-J. Peng, R. Zhang, J. Xie, J.-Q. Huang, Q. Zhang, Adv. Energy Mater. 8 (2018) 1800849.
[82] Z. Liang, D. Lin, J. Zhao, Z. Lu, Y. Liu, C. Liu, Y. Lu, H. Wang, K. Yan, X. Tao, Y. Cui, PNAS. 113 (2016) 2862.
[83] H. Zhang, X. Liao, Y. Guan, Y. Xiang, M. Li, W. Zhang, X. Zhu, H. Ming, L. Lu, J. Qiu, Y. Huang, G. Cao, Y. Yang, L. Mai, Y. Zhao, H. Zhang, Nat. Commun. 9 (2018) 3729.
[84] R. Akolkar, R.M. Sankaran, J. Vac. Sci. Technol. A 31 (2013) 050811.
[85] Y.Y. Wang, Z.J. Wang, D.N. Lei, W. Lv, Q. Zhao, B. Ni, Y. Liu, B.H. Li, F.Y. Kang, Y.B. He, ACS Appl. Mater. Inter. 10 (2018) 20244–20249.
[86] J. Jeong, J. Park, Y. Lee, M. Oh, M.-H. Ryou, Y.M. Lee, Adv. Mater. Interfaces 3 (2016) 1600140.
[87] Q. Li, B.G. Quan, W.J. Li, J.Z. Lu, J.Y. Zheng, X.Q. Yu, H. Li, Nano Energy 45 (2018) 463–470.
[88] M.-H. Ryou, Y.M. Lee, Y. Lee, M. Winter, P. Bieker, Adv. Funct. Mater. 25 (2015) 834–841.
[89] D. Aurbach, E. Zinigrad, Y. Cohen, H. Teller, Solid State Ionics 148 (2002) 405–416.
[90] S.K. Kong, B.K. Kim, W.Y. Yoon, J. Electrochem. Soc. 159 (2012) A1551–A1553.
[91] F. Shen, F. Zhang, Y.J. Zheng, Z.Y. Fan, Z.H. Li, Z.T. Sun, Y.Y. Xuan, B. Zhao, Z.Q. Lin, X.C. Gui, X.G. Han, Y.H. Cheng, C.M. Niu, Energy Storage Mater. 13 (2018) 323–328.
[92] D.-J. Yoo, A. Elabd, S. Choi, Y. Cho, J. Kim, S.J. Lee, S.H. Choi, T.-W. Kwon, K. Char, K.J. Kim, A. Coskun, J.W. Choi, Adv. Mater. 31 (2019) 1901645.
[93] X.H. Zhou, W.J. Huang, C.G. Shi, K. Wang, R. Zhang, J.C. Guo, Y.F. Wen, S.J. Zhang, Q. Wang, L. Huang, J.T. Li, X.D. Zhou, S.G. Sun, ACS Appl. Mater. Inter. 10 (2018) 35296–35305.
[94] H. Wang, Y. Li, Y. Li, Y. Liu, D. Lin, C. Zhu, G. Chen, A. Yang, K. Yan, H. Chen, Y. Zhu, J. Li, J. Xie, J. Xu, Z. Zhang, R. Vilá, A. Pei, K. Wang, Y. Cui, Nano Lett. 19 (2019) 1326–1335.
[95] X.-B. Cheng, H.-J. Peng, J.-Q. Huang, R. Zhang, C.-Z. Zhao, Q. Zhang, ACS Nano 9 (2015) 6373–6382.
[96] R. Mukherjee, A.V. Thomas, D. Datta, E. Singh, J.W. Li, O. Eksik, V.B. Shenoy, N. Koratkar, Nat. Commun. 5 (2014) 3710.
[97] T. Wang, R.V. Salvatierra, A.S. Jalilov, J. Tian, J.M. Tour, ACS Nano 11 (2017) 10761–10767.
[98] K.Y. Xie, W.F. Wei, K. Yuan, W. Lu, M. Guo, Z.H. Li, Q. Song, X.R. Liu, J.G. Wang, C. Shen, ACS Appl. Mater. Inter. 8 (2016) 26091–26097.
[99] C.-Z. Zhao, P.-Y. Chen, R. Zhang, X. Chen, B.-Q. Li, X.-Q. Zhang, X.-B. Cheng, Q. Zhang, Sci. Adv. 4 (2018) eaat3446.
[100] X.B. Cheng, H.J. Peng, J.Q. Huang, F. Wei, Q. Zhang, Small 10 (2014) 4257–4263.
[101] K. Shen, Z. Wang, X. Bi, Y. Ying, D. Zhang, C. Jin, G. Hou, H. Cao, L. Wu, G. Zheng, Y. Tang, X. Tao, J. Lu, Adv. Energy Mater. 9 (2019) 1900260.
[102] W. Guo, S. Liu, X. Guan, X. Zhang, X. Liu, J. Luo, Adv. Energy Mater. 9 (2019) 1900193.
[103] B.W. Byles, N.K.R. Palapati, A. Subramanian, E. Pomerantseva, APL Mater 4 (2016) 046108.
[104] X.-B. Cheng, C. Yan, X.-Q. Zhang, H. Liu, Q. Zhang, ACS Energy Lett. 3 (2018) 1564–1570.
[105] C. Zhan, T. Wu, J. Lu, K. Amine, Energy Environ. Sci. 11 (2018) 243–257.
[106] C. Brissot, M. Rosso, J.N. Chazalviel, S. Lascaud, J. Power Sources 94 (2001) 212–218.
[107] M. Rosso, T. Gobron, C. Brissot, J.N. Chazalviel, S. Lascaud, J. Power Sources 97 (2001) 804–806.
[108] R. Akolkar, J. Power Sources 232 (2013) 23–28.
[109] K.M. Nishikawa, T. Mori, T. Nishida, Y. Fukunaka, M. Rosso, J. Electroanal. Chem. 661 (2011) 84–89.
[110] Z.L. Liang, D., J. Zhao, Z. Lu, Y. Liu, C. Liu, Y. Lu, H. Wang, K. Yan, X. Tao, Y. Cui, Proc. Natl. Acad. Sci. U.S.A. 113 (2016) 2862–2867.
[111] J. Wang, H. Wang, J. Xie, A. Yang, A. Pei, C.-L. Wu, F. Shi, Y. Liu, D. Lin, Y. Gong, Y. Cui, Energy Storage Mater. 14 (2018) 345–350.
[112] H. Liu, X. Chen, X.-B. Cheng, B.-Q. Li, R. Zhang, B. Wang, X. Chen, Q. Zhang, Small Methods 0 (2018) 1800354.
[113] X. Chen, X.-R. Chen, T.-Z. Hou, B.-Q. Li, X.-B. Cheng, R. Zhang, Q. Zhang, Sci. Adv. 5 (2019) eaau7728.
[114] B.-Q. Li, X.-R. Chen, X. Chen, C.-X. Zhao, R. Zhang, X.-B. Cheng, Q. Zhang, Research 2019 (2019) 4608940.
[115] M. Chen, J. Zheng, O. Sheng, C. Jin, H. Yuan, T. Liu, Y. Liu, Y. Wang, J. Nai, X. Tao, J. Mater. Chem. A 7 (2019) 18267–18274.
[116] C. Niu, H. Pan, W. Xu, J. Xiao, J.-G. Zhang, L. Luo, C. Wang, D. Mei, J. Meng, X. Wang, Z. Liu, L. Mai, J. Liu, Nat. Nanotechnol. 14 (2019) 594.
[117] W. Liu, Y.Y. Mi, Z. Weng, Y.R. Zhong, Z.S. Wu, H.L. Wang, Chem. Sci. 8 (2017) 4285–4291.
[118] X. Zhang, R. Lv, A. Wang, W. Guo, X. Liu, J. Luo, Angew. Chem. Int. Edit. 57 (2018) 15028–15033.
[119] Z. Liang, G.Y. Zheng, C. Liu, N. Liu, W.Y. Li, K. Yan, H.B. Yao, P.C. Hsu, S. Chu, Y. Cui, Nano Lett. 15 (2015) 2910–2916.
[120] Z.G. Zhang, Z. Peng, J.Y. Zheng, S.S. Wang, Z.X. Liu, Y.J. Bi, Y.S. Chen, G. Wu, H. Li, P. Cui, Z.Y. Wen, D.Y. Wang, J. Mater. Chem. A 5 (2017) 9339–9349.
[121] R. Zhang, X. Chen, X. Shen, X.-Q. Zhang, X.-R. Chen, X.-B. Cheng, C. Yan, C.-Z. Zhao, Q. Zhang, Joule 2 (2018) 764–777.
[122] W. Luo, Y.H. Gong, Y.Z. Zhu, Y.J. Li, Y.G. Yao, Y. Zhang, K. Fu, G. Pastel, C.F. Lin, Y.F. Mo, E.D. Wachsman, L.B. Hu, Adv. Mater. 29 (2017) 1606042.
[123] K. Fu, Y.H. Gong, Z.Z. Fu, H. Xie, Y.G. Yao, B.Y. Liu, M. Carter, E. Wachsman, L.B. Hu, Angew. Chem. Int. Edit. 56 (2017) 14942–14947.
[124] H. Ye, Z.-J. Zheng, H.-R. Yao, S.-C. Liu, T.-T. Zuo, X.-W. Wu, Y.-X. Yin, N.-W. Li, J.-J. Gu, F.-F. Cao, Y.-G. Guo, Angew. Chem. Int. Edit. 58 (2019) 1094–1099.
[125] Q.D. Sun, W. Zhai, G.M. Hou, J.K. Feng, L. Zhang, P.C. Si, S.R. Guo, L.J. Ci, ACS Sustain Chem. Eng. 6 (2018) 15219–15227.
[126] L. Qin, H. Xu, D. Wang, J. Zhu, J. Chen, W. Zhang, P. Zhang, Y. Zhang, W. Tian, Z. Sun, ACS Appl. Mater. Interfaces 10 (2018) 27764–27770.
[127] C. Jin, O. Sheng, J. Luo, H. Yuan, C. Fang, W. Zhang, H. Huang, Y. Gan, Y. Xia, C. Liang, J. Zhang, X. Tao, Nano Energy 37 (2017) 177–186.
[128] Y. Zhang, W. Luo, C. Wang, Y. Li, C. Chen, J. Song, J. Dai, E.M. Hitz, S. Xu, C. Yang, Y. Wang, L. Hu, Proc. Natl. Acad. Sci. U. S. A. 114 (2017) 3584–3589.
[129] L. Tang, R. Zhang, X. Zhang, N. Zhao, C. Shi, E. Liu, L. Ma, J. Luo, C. He, J. Mater. Chem. A (2019), doi:10.1039/C9TA06401J.
[130] B. Yu, T. Tao, S. Mateti, S. Lu, Y. Chen, Adv. Funct. Mater 28 (2018) 1803023.
[131] C. Zhang, W. Lv, G. Zhou, Z. Huang, Y. Zhang, R. Lyu, H. Wu, Q. Yun, F. Kang, Q.-H. Yang, Adv. Energy Mater. 8 (2018) 1703404.

[132] S. Wu, Z. Zhang, M. Lan, S. Yang, J. Cheng, J. Cai, J. Shen, Y. Zhu, K. Zhang, W. Zhang, Adv. Mater. 30 (2018) 1705830.
[133] K. Huang, Z. Li, Q. Xu, H. Liu, H. Li, Y. Wang, Adv. Energy Mater. 9 (2019) 1900853.
[134] B. Hong, H. Fan, X.-B. Cheng, X. Yan, S. Hong, Q. Dong, C. Gao, Z. Zhang, Y. Lai, Q. Zhang, Energy Storage Mater. 16 (2019) 259–266.
[135] J. Li, P. Zou, S.W. Chiang, W. Yao, Y. Wang, P. Liu, C. Liang, F. Kang, C. Yang, Energy Storage Mater. (2019), doi:10.1016/j.ensm.2019.06.019.
[136] Y. Cheng, X. Ke, Y. Chen, X. Huang, Z. Shi, Z. Guo, Nano Energy 63 (2019) 103854.
[137] J. Pu, J. Li, K. Zhang, T. Zhang, C. Li, H. Ma, J. Zhu, P.V. Braun, J. Lu, H. Zhang, Nat. Commun. 10 (2019) 1896.